EEG Phase Slips Reveal Detailed Brain Activity Patterns of Novice Vipassana Meditators During Decision Making Tasks

Ratna Jyothi Kakumanu[1¶], Ajay Kumar Nair[2¶], Arun Sasidharan[3], Rahul Venugopal[3], Ravindra P Nagendra[3]*, Bindu Kutty[3], Ceon Ramon[4, 5]*

1. Innovation Incubator Inc., Manhasset Hills, NY 11040, USA
2. Center for Brain and Mind (CBM), Department of Psychiatry, National Institute of Mental Health and Neuro Sciences (NIMHANS), Bengaluru, Karnataka, India.
3. Center for Consciousness Studies (CCS), Department of Neurophysiology, National Institute of Mental Health and Neuro Sciences (NIMHANS), Bengaluru, Karnataka, India
4, 5 Department of Electrical and Computer Engineering[4] and Regional Epilepsy Center[5], University of Washington, Seattle, WA 98195, U.S.A.

Ratna Jyothi Kakumanu	jyothi.maanu@gmail.com	ORCID: 0000-0003-3918-2772
Ajay Kumar Nair	ajay.nimhans@gmail.com	ORCID: 0000-0003-3892-6979
Arun Sasidharan	arunsasi84@gmail.com	ORCID: 0000-0001-7090-2315
Rahul Venugopal	rahul.nimhans@gmail.com	ORICID: 0000-0001-5348-8845
Ravendra P Nagendra	ravindrapinna@gmail.com	ORCID: 0000-0002-8243-8684
Bindu Kutty	bindu.nimhans@gmail.com	ORCID: 0000-0001-7483-9675
Ceon Ramon	ceon@uw.edu, ceon@u.washington.edu	ORCID: 0000-0001-8675-613X

* Corresponding authors for publication: Ravindra P Nagendra, Ceon Ramon
* Corresponding author for review: Ceon Ramon. ceon@uw.edu, ceon@u.washington.edu

¶ These authors contributed equally to this work

Short Title: EEG phase slips for Novice Vipassana Meditators

---

	yyyy-mm-dd	
Revision 0:	2025-09-05	(Original Submission)

Abstract

Our study adopted a novel approach, utilizing four biomarkers, namely EEG potentials, their first-order derivatives, and phase slip rates derived from each, to discern the differences between novice Vipassana (NVP) subjects and non-meditator controls (NMC). Phase slip rates are discontinuities in instantaneous phase that represent cortical phase transitions, indicating a significant change in the overall brain state. We employed 128-channel EEG data from eight NMC and eight NVP subjects, collected during a gamified protocol, to investigate object identification within a visual oddball paradigm. EEG was continuously acquired during the first 50 trials for each subject. We retained 44 artifact-free trials per subject (the minimum common across all subjects) and computed within-subject averages. The EEGs were then averaged over NMC and NVP subjects. The EEG was filtered in the alpha band, and the phase was extracted using the Hilbert transform, unwrapped, and the phase slip rates were computed. A montage layout of electrodes was used to make the spatiotemporal plots of biomarkers. Our findings revealed that the spatiotemporal profiles of all four biomarkers differed significantly between the two groups of subjects. Furthermore, the NVP subjects demonstrated faster object recognition. These results not only provide a unique method to use phase slip rates to quantify cognitive differences between NMC and NVP subjects but also present a promising set of biomarkers for quantitative task-based EEG analyses.

Keywords: EEG phase slips, Cortical Phase Transitions, EEG derivatives, Vipassana EEG, Phase Slip Biomarkers, Meditation.

55 **Abbreviations**

56

57 EEG	Electroencephalogram or Electroencephalography
58 EEG′	First order derivative (*d/dt*) of EEG
59 NMC	Non-Meditator Controls
60 NVP	Novice Vipassana
61 RDM*	Relative Difference Measure
62 PSR	Phase Slip Rate or Phase Slip Rates
63 PSR1	Phase Slip Rate extracted from EEG
64 PSR2	Phase Slip Rate extracted from EEG′
65 Poststimulus+	Combined duration of stimulus and poststimulus period

66

67

68 **A. Introduction**

69

70 Phase slips derived from the EEG, a critical biomarker, have been extensively studied to
71 understand cortical neurodynamics under various conditions. These conditions include visual
72 object naming tasks, insight moments [1], dynamics of epileptic seizure evolutions [2], and the
73 formation of propagating spatiotemporal phase cone structures on the cortical surfaces [2, 3]. In
74 all of these studies, there is often additional information about the cortical activity not seen in the
75 power spectral density or phase synchronization analysis of EEG data. Our objective in the
76 present study is to investigate whether additional information can be derived from phase slips

extracted from the EEG of meditative subjects, particularly for novice Vipassana (NVP) subjects in decision-making tasks. Our results indicate that this approach is feasible, offering a promising avenue for future research in meditation and EEG data analysis.

Phase slips are generally extracted from the EEG data using Hilbert transform techniques. Phase slips are generally extracted from the EEG data using Hilbert transform techniques. However, we have recently demonstrated that these phase slips can also be extracted from the derivatives of EEG data [4], which provides additional information about cortical neurodynamics compared to the phase slips extracted from EEG alone. Here we have written the first order derivative (d/dt) of EEG as EEG′. The phase slip rates extracted from EEG are written as PSR1, and those extracted from EEG′ as PSR2. In the present study, we examined the spatiotemporal behavior of four quantities, viz., EEG, EEG′, PSR1, and PSR2 of novice Vipassana (NVP) meditation subjects and compared them with the spatiotemporal behavior of non-meditator control (NMC) subjects. As summarized in the abstract, our results indicate there are quantifiable differences between NMC and NVP subjects. In addition, we examined the different stages of visual object recognition between NMC and NVP subjects, as well as the time it takes to recognize an object. A detailed analysis of N1, P1, and P2 visual evoked potentials [5] and their corresponding phase slip rates was performed, and there were noticeable differences between NMC and NVP subjects. The insight moments are also called ‘Eureka’ moments when one recognizes an object or spontaneously finds a solution to a problem [1, 6]. To our knowledge, these results are new and open a new way to quantify the effects of meditation on cortical neurodynamics by use of biomarkers based on phase slip rates, such as PSR1 and PSR2.

In the following sections, we provide a brief overview of the necessary background material on cortical phase transitions, phase slips, Vipassana meditation, and insight moments, which will help clarify our methods and results. Details of the methods, results, and discussions are presented in the subsequent sections.

B. Background Material

B.1 Criticality, Phase Transitions, and Phase Slips

Criticality refers to the condition of a system that is finely balanced between order and disorder such that a small perturbation can yield large effects [7]. The sudden large shift in the state of the system is called a phase transition. An example of the critical point is the triple point (273.16 Kelvin, 611.73 Pascal) of water, where it can exist in all three phases of solid, liquid, and gas, and a slight change in the temperature or pressure could cause a shift from one state to the other, e.g., from solid to liquid, etc. Other examples of criticality and phase transitions in nature include superconductivity, ferromagnetism, neuronal activity, and swarm technology [8, 9]. Another typical example of self-organized criticality is the sandpile model [10, 11], where one continually adds sand to a vertical pile until it collapses, triggering cascading avalanches.

Phase slips are discontinuities in rhythmic activity [12, 13] and arise due to the shift from the coordinated synchronous rhythmic activity to more independent asynchronous firing of a group of neurons in the cortex. This generally happens at mesoscopic scales in the brain, but could also

occur at larger interconnected areas in the whole brain. The short (i.e., local) and the long (i.e., global) range electrical interconnections in the brain happen over the white matter fiber pathways. Due to these interconnected regions, one can observe phase slips in the invasive ECoG (Electrocorticogram) recordings and noninvasive EEG (Electroencephalogram) recordings. These phase slips represent cortical phase transitions, indicating a significant change in the overall brain state. These changes in brain states could be related to cognitive processes, such as learning or memory, or changes in internal or external stimuli [1, 13]. Examples of internal stimuli include a shift in attention or a change in an internal thought process. Examples of external stimuli include audio or visual stimuli, temperature, pressure, or even social interactions. All of these could cause a phase transition leading toward the formation of a phase slip.

Phase transitions in the brain occur because the electrical activity of the whole cortex is generally in a metastable state, very close to a critical point, and a slight disturbance could cause a phase transition [14, 15]. The phase transitions produce bursts of neural oscillations, which show up as small perturbations in the EEG, MEG, or ECoG data, which becomes a site for the formation of phase slips. Most of these behaviors of criticality in nature can be modeled with an Ising model of ferromagnetism, which has also been applied to the modeling of avalanches in networked neurons [16]. Some other models based on nonlinear many-body field dynamics have also been proposed for the formation of phase slips at mesoscopic scales in the brain [13, 17, 18]. Thus, in summary, one can consider phase slips as a reliable biomarker to study brain behavior, which has been applied to study the cognitive behavior of the brain from EEG [1] and localization of epileptogenic sites from ECoG [3] and EEG [19] data. In the present report, we are applying

143 these phase slip techniques to study the cognitive behavior of novice Vipassana subjects during
144 decision-making processes.
145
146 **B.2 Vipassana Meditation and Brain Processes**
147
148 Vipassana meditation, as outlined in the Pāli Canon, is rooted in the direct experience of the
149 Buddha and the precise method he used to attain enlightenment. As such, it occupies a central
150 place in Buddhist teachings. Vipassana is a comprehensive system of mental cultivation and a
151 transformative process aimed at elevating consciousness [20]. In contemporary neuropsychology,
152 Vipassana is often equated with "mindfulness" and has been widely adopted as a clinical
153 intervention for managing emotional distress, maladaptive behaviors, and psychosomatic
154 conditions [21]. An expanding body of research highlights its efficacy in enhancing
155 psychological and physical well-being [22, 23], making it one of the most extensively studied
156 psychotherapeutic practices globally. The practice has attracted increasing interest in
157 neuroscience for its potential to foster cognitive flexibility, emotional regulation, and
158 psychological resilience [24, 25].
159
160 Despite the growing empirical interest, many studies have neglected the underlying philosophical
161 context of meditation and its broader implications for consciousness and well-being [26].
162 Moreover, existing research often centers on Western adaptations of Vipassana. Studies on
163 incarcerated populations completing the traditional 10-day courses have found reduced
164 recidivism, depression, anxiety, hostility, and substance use [27]. Studies among experienced

165 Vipassana practitioners in the classical tradition of Sayagyi U Ba Khin, as taught by S.N.
166 Goenka, have identified proficiency-specific psycho-neural correlates of well-being [28, 29].
167 This tradition aims at a radical transformation of consciousness through a sequence of three
168 interdependent meditative techniques designed to accommodate a wide range of temperaments
169 while maintaining internal coherence (Fig. 1).
170
171 ----------
172 Fig. 1. Schematic representation of the Vipassana practice in the tradition of Sayagyi U Ba Khin
173 as taught by S.N. Goenka.
174 ----------
175
176 The training begins with Ānāpāna Sati (Focused Attention Meditation), in which attention is
177 anchored to the breath. This practice cultivates sustained attention, heightened awareness, and
178 perceptual acuity while reducing habitual mind-wandering [30].
179
180 Next, during Vipassana Bhāvanā (Insight Meditation, Mindfulness or Open Monitoring
181 Meditation), practitioners learn to experience the phenomena within the mind-body continuum
182 with objective awareness. These phenomena, including thoughts and feelings, both pleasant and
183 unpleasant, are seen as transient, insubstantial, and ultimately dissatisfactory. Through this
184 sustained, non-reactive observation, the practitioner gains direct insight into the impermanent
185 and impersonal nature of phenomena. Over time, one learns to disidentify from habitual

responses of craving and aversion, seen as sources of suffering, and begins to experience increasing inner stability and self-mastery [30, 31, 32].

Finally, Mettā Bhāvanā (Loving-Kindness/Compassion Meditation) involves the deliberate cultivation and radiance of goodwill toward oneself and all beings, free from bias or reservation. This phase helps dissolve self-centered patterns and reinforce the equanimity gained through Vipassana, supporting the integration of insight into daily life [30]. Throughout Mettā practice, the practitioner maintains an objective stance, extending compassionate awareness without expectation.

These three practices are not discrete but are interwoven, each reinforcing the others in a unified framework for inner transformation [33]. Taken together, they engage cognitive, affective, attitudinal, and ethical dimensions, forming a deeply introspective and socially relevant practice [20].

B.3 Insight Moments and Visual Evoked Potentials

Insight moments are also called 'Aha!' or 'Eureka' moments, which relate to suddenly or spontaneously finding a solution to a problem. A well-known example is the famous ‘Eureka' moment of Archimedes. The ‘Eureka' moment is part of the four stages of creativity suggested by Graham Wallas in 1926, which are commonly called: Preparation, Incubation, Illumination, and Verification [34, 35, 36]. Illumination is the ‘Eureka' moment. These insight moments can be

studied with EEGs, either in the resting state or in evoked response potentials studies, such as looking at a picture on a computer screen while collecting the EEG data [1, 6, 37, 38, 39].

The prominent peaks of visual evoked potentials, P1, N1, and P2, are integral to insight moments, which are generally observed within the first 300 ms from the start of the stimulus onset. After that, within the 0.3 s to 1.2 s time frame from the stimulus onset, several other prominent peaks are also related to different stages of insight moments, allowing the subject to recognize the name, shape, and form of the object on the computer screen and compare them with what is stored in the subject's memory [1]. Thus, analysis of spatial profiles of EEG and phase slip rates for these peaks and their differences between NMC and NVP subjects is an important topic of investigation. An interesting observation from our results was that there was no remarkable difference in the latency of P1, N1, and P2 peaks for the NMC and NVP subjects. However, there were some noticeable differences in the spatial profiles of these peaks for NMC and NVP subjects. More details are given in the results section.

C. Materials and Methods

C.1 Data Collection Protocols

High-density EEG data of 16 healthy adult participants (8 NMC, 8 NVP) were used in this study. Their data sets were previously collected as part of a larger study [28. 29] at the National Institute of Mental Health and Neurosciences (NIMHANS), Bangalore, in accordance with the approved

guidelines for human subjects research. A 128-channel EGI system (Electrical Geodesics, Inc., Eugene, OR, USA; now part of Magstim Inc., 1626 Terrace Dr, Roseville, MN 55113) was used for the data collection. Details on the task parameters have been previously reported [40]. In brief, participants engaged in 'ANGEL', a gamified audiovisual oddball task with three levels of complexity, presented in 16 blocks each. The first two blocks of data from the second level ('Whodunnit'), comprising of 50 trials were used for the present study. Each block had a salient image (black and white face, shape, or a distorted image) presented on one side of a fixation sign, and a non-salient image (black and white checkerboard) presented on the other side. Further, images of one salient image type were presented frequently on one side in a block (for example, a face presented on the right of the fixation) and represented the 'frequent' condition. About 20% of the time ('rare' trial condition), a salient image of one of the other three image types was presented on the other side (for example, shape to the left of the fixation). Participants were asked to press one of two buttons to indicate if the salient image appeared on the left or the right of the fixation. Figure 2 shows an example of the sequence of images.

Fig. 2. Protocol Diagram from earlier publication. Representative examples of two types of task blocks. (From Nair et al., 2016).

C.2 Preprocessing of the EEG Data

252 We used MATLAB (MathWorks Inc., Natick, MA, USA) and EEGLAB software 41] for
253 preprocessing the EEG data, phase slip computations, and visualization of results. The data was
254 filtered with an equiripple filter in a 3–49 Hz broadband and then re-referenced to the common
255 averaged reference. The upper frequency of 49 Hz was selected to eliminate the contamination
256 from the power-line frequency of 50 Hz in India, where the data sets were collected. Using the
257 ICA (independent component analysis) techniques, the muscle, eyeblink, and heartbeat artifacts
258 were removed and then referenced to the common average reference. After that, the data were
259 averaged over trials for each subject. For one subject, we found 44 good trials out of 50. For
260 consistency, we chose 44 good trials out of 50 for all subjects. The averaged trials for eight NMC
261 and eight VPN subjects were averaged. This way, at the end, we had one grand-averaged data set
262 for NMC subjects and another similar data set for NVP subjects. These data sets were then
263 referenced to the common averaged reference for each channel, filtered in the alpha (7–12 Hz)
264 band with an equiripple filter, and then used for phase slip extraction and PSR computations.
265
266 An example of the EEG data after preprocessing is shown in Fig. 3. It is only for two electrodes,
267 one in the frontocentral area (Fig. 3A) and the other in the right visual area (Fig. 3B). Their
268 spatial location is shown in Fig. 3C. The periods of prestimulus, stimulus, and poststimulus
269 period are marked on the top of the EEG plot in Fig. 3A. For analysis and display the time scale
270 for the prestimulus period is -1.0 s to 0.0 s, for the stimulus period is from 0.0 s to 0.240 s, and
271 for the poststimulus period is from 0.240 s to 2.0 s, respectively. The prestimulus period is also
272 commonly referred to as the baseline period. Additionally, we use the terminology

'poststimulus+' to refer to the combined duration of the stimulus and poststimulus period from 0.0 s to 2.0 s.

Fig. 3. An example of an EEG trace after preprocessing for two electrodes in a 3-49 Hz broadband. (A) EEG from one of the electrodes in the frontocentral area, (B) EEG from one of the electrodes in the right visual area, and (C) spatial profile of EEG potentials at the P1 peak of the NVP subject. Note that the time series profiles of PSRs at two electrodes are significantly different during the 0.0-1.0 s period, when the subject is visualizing and analyzing the image of the object during covert object naming tasks.

The EEG plot of the right visual electrode (Fig. 3B) has three prominent peaks marked as P1, N1, and P2, which are typical visual event-related potentials [5] observed when one begins to look at an object. It is part of the perception cycle during the stimulus period. The same peaks are also marked in Fig. 3A for the frontocentral electrode. Notice that the polarity of the peaks is reversed in Fig. 3A compared to Fig. 3B. For simplicity, we will use the positive and negative nomenclature of the peaks from the visual electrode in Fig. 3B.

An interesting feature is that these peaks for NMC and NVP subjects are very close. This would suggest two things. First, our data collection and stimulus protocol are robust, so the data collected over several days does not smear the prominent peaks in the EEG data. The second

295 point is that the initial response of the brain to a visual stimulus is very similar in NMC and NVP
296 subjects. For the NVP subjects, these P1, N1, and P2 peaks are located at 115 ms, 214 ms, and
297 303 ms, respectively, from the start of the stimulus period at 0.0 s. The location of these peaks
298 for the NMC subjects is at 122 ms, 190 ms, and 305 ms, respectively.
299
300 During the period of 0.4 to 1.0 s, there are several prominent peaks with different locations are
301 observed for NMC and NVP subjects. These peaks belong to the various stages of the insight
302 moments [1, 37] related to the decision-making and object recognition processes, such as
303 searching for the name and form of the object in the memory [1]. These insight moments are also
304 called "Aha" moments or "Eureka" moments, and can be studied during both the stimulus period
305 [6] and/or during the poststimulus period [1, 42, 43]. A detailed analysis of these insight
306 moments for NMC and NVP subjects is given in the Results section.
307
308 A note about the spatial plot in Fig. 3C, which will also apply to subsequent spatial plots. The
309 head circle represents the largest possible diameter of the head, as seen from the top, and it
310 covers most of the electrodes on top of the head, positioned slightly above the level of the
311 eyebrows. In addition, there are several lower-level electrodes positioned around the head, which
312 are located below the eyebrows and extending down to ear level. The electrical activity on these
313 electrodes is shown outside the head circle, and electrical activity will be picked up from the
314 lower, i.e., inferior, and deeper parts of the brain. There are some electrodes on the forehead,
315 whose electrical activity will be included outside the head circle above the nose in spatial plots.

A few of the electrodes on the face are not included in the spatial plots. More details about this can be inferred from the topographic plot script (topoplot.m) included in the EEGLAB software.

C.3 Phase Slip Rate Computations

The procedures to compute PSR are described in our previous studies [1, 4]. Similar procedures have been used here. The sawtooth patterns of the phase were extracted from the EEG data using the Hilbert transform, which, on unwrapping and detrending, shows phase slips at the locations of small perturbations in the EEG data related to cortical phase transitions. A pictorial representation of phase slip extraction from EEG and its first derivative is given in Fig. 4. It shows the EEG and its first order derivative, EEG′ from one of the electrodes in the front central area, sawtooth pattern of the phase, unwrapped phase with one of the large episodic phase shifts, and several of the large sharp and small broad phase slips. Our interest will be only in the phase slips in the alpha band of 7-12 Hz, and, thus, larger phase slips will not be counted in PSR computations. The PSR1 is from the EEG, and the PSR2 is from the first derivative of the EEG, respectively. Here, EEG voltage is represented as a time series data: $y = y_1 + y_2 + ... + y_n$, and y' is (dy/dt) of the time series. The y' was computed by the first order differencing of the time series y and then dividing it by the digitization interval. A similar representation has been used earlier [4, 44].

Fig. 4. A pictorial representation of phase slip extraction steps. Plots in the left column are marked in (A) for the phase slips extraction from the EEG, and, similarly, the right column (B) is for the phase slips extraction from EEG′, i.e., from the first order derivative of EEG. The top row is the EEG and EEG′, the second row from the top is the sawtooth pattern of the phase, the third row from the top is the unwrapped phase, and the bottom row shows some of the phase slips.

The PSR from the phase slips was calculated in a stepping window of 10 ms duration with a step size of one digitization point equal to 1.0 ms based on the sampling rate of 1 kHz. The window size is selected based on the Shanon entropy function [45, 46, 47] such that it is short enough to capture the information (lower entropy) but not wide enough to smear (higher entropy) the information. For our case, a window size of 10 ms will give us a maximum value of PSR of 10 counts/10 ms if there were phase slips at each digitization point. In general, it will be difficult to find phase slips at each digitization point, and thus, PSR will be less than 10 counts in each window. The step size of one digitization point, i.e., 1.0 ms, is 10% of the window size, which provides smooth transitions without smearing the information content in going from one stepping window to the next. Also, this window size is approximately 7% of the time period of the lowest frequency (7 Hz) of interest in the alpha band, and the step size is adequate to avoid aliasing errors due to undersampling.

These procedures were used for computing phase slip rates, PSR1 from the EEG data, and PSR2 from the first order derivative of the EEG data. The spatial plots of EEG, PSR1, and PSR2 were constructed with a montage layout of 128 electrode positions on a flat surface.

To separate the phase slips arising from the biological processes versus the random noise, several criteria were applied, which we have used before [4]. These include: (1) phase slip frequency is within the alpha band of 7–12 Hz, (2) sign of the positive or negative peaks did not change for at least three consecutive time steps, and (3) the magnitude of the three consecutive peaks was within the mean ± 1.05σ of the three peaks, where σ is the standard deviation of the mean. The application of these criteria significantly reduced the counting of phase slips due to random noise, while simultaneously maximizing the counting of phase slips from biological processes.

C.4 Surrogate Data Testing

After filtering in the alpha band, the PSR of random noise was computed from the randomly shuffled EEG data. We used the 'randperm' command in the MATLAB software for this. These techniques have been used before by us [1, 2, 4] and also described in a recent paper [48] on surrogate data analysis. The power spectral density of the randomly shuffled EEG data was significantly different from the original EEG data, and it was close to a white noise. The phase slips were extracted from the randomized EEG data and then randomly shuffled. After that, the PSR1 was computed in a stepping window of 10 ms duration with a step size of one digitization point. The mean and standard deviations of PSR1 were found to be zero after averaging over

n = 100 trials. A similar analysis was also performed on the PSR2 derived from the first order derivatives of the randomly shuffled EEG data. It was found that in this case also, the mean and standard deviations of PSR2 from the shuffled data were zero after averaging over n = 100 trials. This shows that our reported results are from the biological processes extracted from the EEG data and are above the results from the random noise.

C.5 Statistical Analysis

To compare two data sets, we used a paired Student's t-test or histogram distributions. However, these two tests often fail if the means and standard deviations of two distributions are very close to each other. Similarly, the Kolmogorov-Smirnov test also fails if two cumulative distribution functions are similar, even though there are observable and quantifiable differences in their spatial plots. In such situations, the Relative Difference Measure (*RDM**) and the Magnification Factor (*MAG*) are considered to be better choices than the Student's t-test, the Kolmogorov-Smirnov test, or the histogram distribution to compare two spatial plots of similar values [2, 45]. It is a prevalent technique to quantify the differences between two spatial plots of data, such as in EEG spatial plots [2, 45]. Most of our results are spatial plots of EEG or phase slip rates. The *RDM** is defined as:

$$RDM^* = \sqrt{\sum_{j=1}^{m}\left[\frac{Z_k^{RM}}{\sqrt{\sum_{k=1}^{m}\left(Z_k^{RM}\right)^2}} - \frac{Z_k^{TM}}{\sqrt{\sum_{k=1}^{m}\left(Z_k^{TM}\right)^2}}\right]^2} \quad \textbf{(1)}$$

where index, $j=1:m$, runs over all 128 electrodes. The Z_k^{RM} are the values for the reference measurement, and Z_k^{TM} are the values of the test measurements. As an example, it could be the EEG potential at the kth electrode for the reference measurements (RM) and the test measurements (TM), respectively. The magnification factor is defined as:

$$MAG = \frac{\sqrt{\sum_{k=1}^{m}\left(Z_k^{TM}\right)^2}}{\sqrt{\sum_{k=1}^{m}\left(Z_k^{RM}\right)^2}} \qquad \textbf{(2)}$$

The *RDM** is a measure of the difference in spatial profiles of two data sets, and *MAG* is a measure of differences in the magnitude of the two data sets. If two data sets are the same, *RDM** will be zero and *MAG* will be unity. The degree of differences is quantified with higher values of *RDM** in the range of 0.0 to 1.0. The maximum value of *RDM** is 1.0 if the test measurements are zero. The variation in the value of *MAG* from unity will quantify the differences in the magnitude of the two data sets. Values of *MAG* greater than 1.0 would mean that the test measurements (TM) are higher in magnitude as compared with the reference measurements (RM). And the reverse is true if *MAG* is less than 1.0.

To compare the means of more than two data sets, we used ANOVA (Analysis of Variance). Histogram plots of data sets were also made. Mean and standard deviations of two histogram

plots were computed and compared. In addition, two histogram distributions were also compared with their RMS bin count differences, $RMS\ H_{diff}$, defined as:

$$RMS\ H_{diff} = \sqrt{\frac{1}{N}\sum_{i=1}^{N}((H_1(i) - H_2(i))^2} \qquad \textbf{(3)}$$

where H_1 and H_2 are two histogram distributions with N bins.

C.6 Computational Resources

The data analysis was performed on a desktop computer with an 8-core CPU and 112 GB of memory using EEGLAB [41]. For computations of PSR requiring more significant (>112 GB) memory, we used MATLAB software at the UCSD (University of California, San Diego) supercomputing center using their NSG (Neuroscience Gateway) portal.

D. Results

D.1 Non-meditator Control (NMC) Subjects

The temporal plots of EEG, EEG′, PSR1, and PSR2 of one of the electrodes in the front central area are given in Fig. 5. During the stimulus and poststimulus periods, the prominent event-related potential peaks are recognizable in the top left plot of broadband EEG in the 3-49 Hz, which are difficult to see in the alpha band EEG plot, (left and right middle plots). The

prominent peaks in the EEG are difficult to recognize in the plot of the EEG′ (top right plot). They tend to disappear with the first-order differentiation of the EEG. However, the small high-frequency perturbations in the EEG are amplified due to the removal of linear trends through differentiation. In the alpha band, one can see the presence of the alpha wave spindling and small perturbations in the EEG and also in the EEG′.

Fig. 5. Temporal plots of quantities of one of the electrodes in the front central area for non-meditator control (NMC) subjects. (Top left) EEG in 3-49 Hz band, (top right) EEG′ in 3-49 Hz band, (middle left) EEG filtered in the alpha band of 7-12 Hz, (middle right) EEG′ filtered in the alpha band of 7-12 Hz, (bottom left) phase slip rate PSR1 extracted from EEG in the alpha band, and (bottom right) phase slip rate PSR2 extracted from EEG′ in the alpha band. Notice the prominent peaks in PSR1 and PSR2 related to brain activity during the visual object recognition tasks. The prestimulus period is from -1.0 to 0.0 s. The combined stimulus and poststimulus period, referred to as the poststimulus+ period, spans from 0.0 to 2.0 seconds.

The PSR1, computed from the EEG data filtered in the alpha (7-12 Hz) band, provides crucial insights. Notably, the PSR1 plot reveals a small and sharp large peak between -0.9 s and -0.45 s during the prestimulus period. These peaks are associated with the background activity of the brain while looking at the checkerboard pattern during the prestimulus period. The broad peak

during the poststimulus period, stretching from 0.15 s to 0.95 s, with the prominent peak centered at 0.6 s, is equally significant. This peak is related to the initial response of the visual cortex and the recognition of the object in the language and memory areas of the brain, a common occurrence in the insight moment analysis of visual object naming [1]. The broad peak between 1.35 and 1.9 s is probably related to the brain returning to the background activity after the end of visual object naming processes.

The plot of PSR2 reveals the rate of change in the neuronal population participating in the formation of scalp EEG. It exhibits a bifurcated peak between -0.8 and -0.2 s during the prestimulus period, which correlates with the background activity of the brain while viewing the checkerboard pattern. During the first second of the combined stimulus and poststimulus period, a broad peak is observed from 0.0 to 0.8 s, with the main peak at 0.45 s, which is likely related to the recognition of the object in memory and language areas [1, 37]. The several peaks from 1.0 s to 2.0 s correspond to the return to background activity.

The spatial plots of the root mean square (RMS) of EEG and EEG′, and mean values of PSR1 and PSR2 for NMC subjects are given in Fig. 6. These values were computed within a stepping window of 0.5 s covering the period of -1.0 to 2.0 s.

Fig. 6. Spatiotemporal plots of the root mean square (RMS) values of EEG and its first order derivative (EEG′) and their associated mean values of phase slip rates for non-meditator

control (NMC) subjects. The RMS and mean values were computed within a 0.5 s stepping window. The temporal duration for each frame is given at the top. (A) The top two rows are for the RMS EEG and the mean PSR1, respectively. (B) The bottom two rows are for the RMS EEG′ and the mean PSR2. Notice the shifting spatial patterns of all four quantities.

Fig. 6 is divided into sections (A) and (B). The top two rows in section (A) present the spatial plots of RMS EEG and the mean values of associated phase slip rate, i.e., mean of PSR1 (#/(10 ms)), respectively. The RMS and mean values were computed within a 0.5-s stepping window. Similarly, the bottom two rows marked as section (B) are the spatial plots of the RMS value of the first-order derivative of EEG, i.e., EEG′, and the mean values of its associated phase slip rate, PSR2 (#/(10 ms)), respectively. The frame numbers and their temporal durations are given at the top. The first two frames, i.e., Frame 1 and Frame 2, are during the prestimulus period. The Frame 3 from 0.0 s to 0.5 s is for the combined period of stimulus (0.0 to 0.240 s) and part of the poststimulus (0.240 s to 0.5 s) period. The remaining three frames are for the poststimulus period.

In all frames, RMS EEG activity is intense in the forehead area above the nasion point, corresponding to the brain activity in the brain's frontal area responsible for the emotional responses to external stimuli, such as visual images on the computer screen. In Frame 1 and Frame 2, it is subdued, begins to increase in Frame 3, and becomes strongest in Frame 4. After

that, it starts to decrease in subsequent Frames 5 and 6. There is another activity spot in the left frontocentral area, which is present in all six frames. It is of moderate strength (0.2 μV) during the prestimulus period but becomes stronger during the poststimulus period, with the most substantial value of 0.3 μV in Frame 4. The mean PSR1 plots (Fig. 6A, bottom row) differ from RMS EEG plots. There is a bright spot near the right ear in the central right temporal area. It is present during the stimulus period and also during the poststimulus period. Its activity is noticeable in Frames 3 to 4 during the poststimulus period and almost disappears in Frame 6. There is also an active spot in the right frontocentral area, located just to the right side, below the nose. The activity at this spot is high in Frames 3 and 4, which matches the several peaks of event-related potentials in the EEG during this period (Fig. 5, top left plot). An interesting feature to note is that mean PSR1 activity is widespread in the lower half of the plot, with some areas in the central and parietal regions, as well as others near the left and right edges of the plot. The electrodes located below the skull capture the electrical activity from the deeper areas of the brain, including the thalamus and amygdala. These corresponding features are not visible in the plots of the RMS EEG.

The spatial plots of RMS EEG′ and the corresponding mean PSR2 are given in Fig. 6B. The spatial features in RMS EEG and RMS EEG′ are very similar, which is expected because EEG′ is the first order derivative of the EEG. Similarly, the spatial patterns of mean PSR2 are similar to those of mean PSR1, representing the rate of change of the neuronal population involved in cortical electrical activity.

526 A one-way ANOVA analysis was performed on the six frames of RMS EEG, and it was found
527 that the mean of all six frames were significantly ($p < 0.01$) different from each other. A similar
528 analysis was performed on the remaining three quantities, namely, RMS EEG′, mean PSR1, and
529 mean PSR2. Results were similar, i.e., the means of the six frames for each quantity were
530 significantly ($p < 0.01$) different from one another. A comparative analysis of the six spatial plots
531 of EEG and PSR1 was done with the paired Student's t-test, and it was found that each frame was
532 significantly ($p < 0.01$) different from the others. A similar analysis was performed on each frame
533 of RMS EEG′ and the mean PSR2, and it was found that they were significantly ($p < 0.01$)
534 different from each other.
535
536 **D.3 Novice Vipassana (NVP) Subjects**
537
538 All quantities related to one of the frontocentral electrodes for NVP subjects are given in Fig. 7.
539 There are well-defined and recognizable peaks in the EEG during the prestimulus, stimulus, and
540 poststimulus periods. During the prestimulus period, the prominent peaks are located at -0.88 s,
541 -0.793 s, and -0.67 s. These peaks are related to the background activity of looking at the
542 checkerboard pattern on the computer screen. During the stimulus and poststimulus periods, the
543 prominent peaks are at: 0.172 s, 0.4 s, 0.56 s, 0.702 s, and 0.903 s. These peaks are related to
544 insight moments [37] for visualization and recognition of the object during the stimulus and
545 poststimulus periods [1]. Their temporal location for NVP subjects differs from that of the NMC
546 subjects. This is also reflected in the plot of PSR1. The prominent peaks are at -0.544 s, 0.436 s,

0.65 s, 0.823 s, and 1.503 s. These plots suggest that the timings for the object recognition steps for NVP subjects are slightly different from those of NMC subjects.

Fig. 7. Temporal plots of quantities of one of the electrodes in the front central area for novice Vipassana (NVP) subjects. (Top left) EEG in 3-49 Hz band, (top right) EEG′ in 3-49 Hz band, (middle left) EEG filtered in the alpha band of 7-12 Hz, (middle right) EEG′ filtered in the alpha band of 7-12 Hz, (bottom left) phase slip rate PSR1 extracted from EEG in the alpha band, and (bottom right) phase slip rate PSR2 extracted from EEG′ in the alpha band. Notice the prominent peaks in PSR1 and PSR2 related to brain activity during the visual object recognition tasks

---

The spatiotemporal plots of brain activity for NVP subjects are given in Fig. 8. These plots are slightly different from the corresponding plots of NMC subjects. There is a bright spot near the nose in the RMS EEG plot in Frame 1. The activity related to the orbital brain is picked up by the electrodes on the forehead above the nasion point. This disappears in the subsequent frames. In Frame 3, there is a large bright spot at the bottom, which relates to the first impressions of the visual stimulus during the stimulus and the start of the poststimulus period. In the following two frames, frames 4 and 5, a low level (~ 0.1 μV) RMS EEG activity is spread in the broader area in the left frontal, central, and left central parietal areas. These are probably related to a search for

the name and form of the stimulus object in the language and memory areas of the brain. Frame 6 represents the return to the brain's background activity while looking at the checkerboard pattern.

Fig. 8. Spatiotemporal plots of the root mean square (RMS) values of EEG and EEG′ and their associated mean values of phase slip rates for novice Vipassana (NVP) subjects. The RMS and mean values were computed in the stepping window of 0.5 s duration. The temporal duration for each frame is given at the top. (A) The top two rows are for the RMS EEG and the mean PSR1, and (B) the bottom two rows are for the RMS EEG′ and the mean PSR2, respectively. Notice the shifting spatial patterns of all four quantities from Frame 1 to Frame 6.

The spatial patterns of mean PSR1 plots are different from the RMS EEG spatial plots. This is particularly noticeable in frames 3, 4, and 5 when the bulk of the brain activity happens to recognize the visual stimuli on the screen. The brain activity is widespread in different parts of the brain and becomes less in Frame 5. In Frame 6, the PSR1 activity is similar to that in Frame 1, signifying that brain activity has returned to the background level at the end of the trial. The spatial patterns of RMS EEG and RMS EEG′ are similar. Similarly, the spatial patterns of mean PSR1 and PSR2 are very similar except in Frame 6. The PSR2 activity has two bright spots, one near the left central temporal area and one in the left posterior area, which are absent in the PSR1 spatial plot.

590 A one-way ANOVA analysis was performed on the six frames of four quantities, viz., RMS
591 EEG, RMS EEG′, PSR1, and PSR2. It was found that the means of all six frames were
592 significantly ($p < 0.01$) different from each other for each of the four quantities. A comparative
593 analysis of the six spatial plots of EEG and PSR1 shown in Fig. 8 for NVP subjects was
594 performed using the paired Student's t-test, and it was found that each frame was significantly
595 different from the others ($p < 0.01$). A similar analysis was performed on each frame of RMS
596 EEG′ and the mean PSR2, and it was found that they were also significantly different from each
597 other ($p < 0.01$).
598
599 **D.3 Differences between NMC and NVP Subjects**
600
601 **D.3.1 EEG and PSR1 Differences between NMC and NVP Subjects**
602
603 The poststimulus+ values above the prestimulus, i.e., baseline values, were computed for the
604 NMC and NVP subjects. For these purposes, the stimulus period of 0 to 240 ms was combined
605 with the poststimulus from 0.24 s to 2.0 s, and it is called the poststimulus+ period. In general,
606 the majority of the brain response happens between 0.04 s and 1.2 s from the start of the visual
607 stimulus at 0.0 s [1]. The RMS EEG was computed for the pre- and poststimulus+ periods
608 separately. Then the prestimulus values were subtracted from the poststimulus+ values to obtain
609 the values above the baseline, i.e., above the prestimulus values. The same procedures were
610 repeated for RMS EEG′, mean PSR1, and PSR2.
611

612 ----------

613 Fig. 9. (A) Spatial plots of RMS EEG above the baseline of NMC and NVP subjects, (B)

614 corresponding spatial plots of mean PSR1 above the baseline, (C) histogram distribution

615 of RMS EEG values shown in spatial plots of A, and (D) histogram distribution of

616 PSR1values shown in spatial plots of B.

617 ----------

618

619 RMS EEG and mean PSR1 above the prestimulus are given in Fig. 9. The spatial plots of RMS

620 EEG are shown in Fig. 9A, and the mean PSR1 are given in Fig. 9B. The left plot is for NMC

621 subjects, and the right plot is for NVP subjects. For NMC subjects, the RMS EEG activity is very

622 strong at the top of the plots, which is from the electrodes on the forehead area and near the eyes.

623 We have removed the artifacts related to eye motion and eye blinks; thus, these electrodes show

624 the activity from the orbital and frontal lobes of the brain. In comparison, the frontal activity is

625 low for NVP subjects. In addition, for NVP subjects, there is more activity outside the head circle

626 in the left temporal areas. Inside the head circle for NMC subjects, there are bright spots in the

627 frontal and left central regions, which are less intense for NVP subjects. The paired Student's

628 t-test showed a significant ($p < 0.01$) difference between the spatial plots of the RMS EEG of

629 NMC and NVP subjects. Similarly, the RDM* and MAG values of 1.36 and 1.04, respectively,

630 suggest some noticeable differences between the two spatial plots. The RDM* of 1.36 would

631 suggest a 36% difference in spatial distribution. The MAG of 1.04 would indicate that there is a

632 4% difference in the magnitude between the two plots. This is very much evident in the

633 differences in the relative magnitude of bright spots at similar locations in the two plots. These

differences are also visible in the histogram plot of Fig. 9C. The mean values of histogram counts are the same for both groups, but the standard deviations, σ, are different. The RMS values of histogram bin counts for NMC and NVP subjects are 22.33 and 19.49 counts, respectively. The RMS values of histogram bin counts for NMC and NVP subjects are 22.33 and 19.49 counts, respectively. The RMS difference of histogram bin counts, RMS H_{diff} is 17.55 counts. This translates to about a 42% difference for the total bin counts, and could be considered a significant difference between the NMC and NVP subjects.

The spatial plots of PSR1 are given in Fig. 9B, and the corresponding histogram distributions are given in Fig. 9D. For NMC subjects, the mean PSR1 is distributed all over the plot. In contrast, for the NVP subjects, it is strong in the left and right temporal areas. Also, a bright spot near the right ear, which does not have a corresponding high activity in the EEG plot. A paired Student's t-test was performed on the absolute values of mean PSR1 for the NMC and NVP subjects, and it was found that they were significantly ($p < 0.05$) different from each other. The *RDM** and *MAG* values are 1.41 and 1.38, which will also suggest that the two plots are significantly different. The mean values of histogram counts of PSR1 are the same for both groups, but the standard deviations, σ, are different. The RMS values of histogram bin counts of PSR1 for NMC and NVP subjects are 20.74 and 18.88 counts, respectively. The RMS difference of histogram bin counts is 6.52 counts. This translates to about a 16% difference when normalized to the total number of bins, and could be considered a noticeable difference in the histogram counts of PSR1 between the NMC and NVP subjects.

656 **D.3.2 EEG′ and PSR2 Differences between NMC and NVP Subjects**

657

658 RMS EEG′, mean PSR2 above the prestimulus values, and their corresponding histogram
659 distributions are given in Fig. 10. For NMC subjects, the RMS EEG′ activity is very strong at the
660 top of the plots, which is from the electrodes on the forehead area and near the eyes. In contrast,
661 for NVP subjects, the RMS EEG′ activity is in the left side temporal regions of the plots. The
662 differences in their spatial distributions are exemplified by the *RDM** value of 1.27, while their
663 magnitudes are very similar, as indicated by the *MAG* value of 1.08. A paired Student's t-test was
664 performed on the RMS EEG′ values for the NMC and NVP subjects, and it was found that they
665 were significantly ($p < 0.01$) different from each other. A histogram distribution of these values
666 are given in Fig. 10C. The mean values of histogram counts are the same for both groups, but the
667 standard deviations, σ, are different. The σ is ±18.56 and ±13.65 for the NMC and NVP subjects,
668 respectively. This translates to about a 26% difference between σ for the NMC and NVP subjects
669 and could be considered a significant difference between the two σ values. The RMS values of
670 histogram bin counts for NMC and NVP subjects are 21.79 counts and 18.21 counts,
671 respectively. The RMS difference of histogram bin counts, RMS H_{diff} is 16.95 counts. This
672 translates to about a 42% difference for the total bin counts, and could be considered a significant
673 difference between the NMC and NVP subjects.

674

675 ----------

676 Fig. 10. (A) Spatial plots of RMS EEG′ above the baseline of NMC and NVP subjects,
677 (B) corresponding spatial plots of mean PSR2 above the baseline, (C) histogram

distribution of the RMS EEG′ values shown in spatial plots of A, and (D) histogram distribution of PSR2 values shown in spatial plots of B.

The spatial plots of PSR2 for the NMC and NVP subjects are given in Fig. 10B. For the NMC subject, the hot spots in PSR2 match fairly well with the hot spots in RMS EEG′. However, there are additional hot spots for the NVP subjects in the right parietal areas, which are absent in the RMS EEG′. A paired Student's t-test failed to show any significant differences between the PSR2 values for the NMC and NVP subjects. However, the *RDM** of 1.34 suggests that spatial distributions of PSR2 are significantly different from each other, as shown in Fig. 10B.

A histogram distribution of PSR2 is given in Fig. 10C. The mean values of histogram counts are the same for both groups, but the standard deviations, σ, are different. The σ is ±11.49 and ±13.10 for the NMC and NVP subjects, respectively. This translates to about a 14% difference between σ for the NMC and NVP subjects. The RMS values of histogram bin counts for NMC and NVP subjects are 16.81 counts and 17.84 counts, respectively. The RMS difference of histogram bin counts, RMS H_{diff} is 5.58 counts. This translates to approximately a 16% difference in total bin counts, which could be considered a slight difference between the NMC and NVP subjects.

D.4 Insight Moments of Object Recognition

EEG potentials in the broad band (3-49 Hz) and the corresponding phase slip rates in the alpha (7-12 Hz) at one of the electrodes in the right visual cortex are presented in Fig. 11. A choice was made to dispaly EEG potentials in the broad band because the P1, N1 and P2 peaks are easily recognizable which are difficult to see in the EEF filtered in the alpha (7-12 Hz) band. For reference, see Fig. 4 for NMC subjects and Fig. 6 for NVP subjects. The visual evoked potential peaks, i.e., P1, N1, and P2, during the stimulus period (0-240 ms) are related to the perception cycle when the subject looks at an object on the computer screen. The latency of these peaks, i.e., the delay between the start of the stimulus (0.0 s) and brain response, is very similar for the NMC and NVP subjects. For NMC subjects, these peaks are located at 122 ms, 190 ms, and 305 ms, respectively. For NVP subjects, these peaks are located at 115 ms, 214 ms, and 303 ms, respectively. Remarkably, these peaks for the two groups of subjects are very close to each other. Here, one group consists of eight NMC subjects, and the other consists of eight NVP subjects.

Fig. 11. EEG potentials in the broad (3-49 Hz) band and corresponding phase slip rates in the alpha (7-12 Hz) at one of the electrodes in the right visual cortex. (Top) EEG potentials with prominent P1, N1, and P2 peaks marked, (middle) corresponding PSR1, and (bottom) corresponding PSR2. Notice the subtle differences in EEG peaks and remarkable differences in PSR1 and PSR2 between NMC and NVP subjects.

---

722 During the poststimulus period (0.24 - 2.0 s), there are also prominent peaks in the EEG related
723 to brain responses while the subject is analyzing and recognizing the name and form of the object
724 [1]. These perception and decision-making processes extend from 0.0 s to about 1.2 s during the
725 stimulus and poststimulus periods. After that, between 1.2 s and 2.0 s, brain activity begins to
726 return to the regular background activity. Here, the background activity is related to a
727 checkerboard pattern, which is displayed during the prestimulus and poststimulus periods. There
728 are several peaks in the EEG during the poststimulus period of 0.0 to 1.2 s, which are at slightly
729 different locations for NMC and NVP subjects, signifying that brain processes are slightly
730 different for the two groups of subjects during the object recognition process.
731
732 The differences between the two groups of subjects are more pronounced when one looks at the
733 temporal patterns of phase slip rates, viz., PSR1 and PSR2, given in the middle and the bottom
734 plots of Fig. 11. The PSR1 is higher for NVP subjects as compared with NMC subjects, while
735 PSR2 has the opposite trend. The PSR2 represents the net rate of number of neurons taking part
736 in the genesis of EEG which one measures at the scalp or subdural electrodes. This suggests that
737 the brain processes of the NMC subjects are changing more rapidly than those of the NVP
738 subjects. One could probably say that the brain processes are more stable and gradually changing
739 for NVP subjects as compared with NMC subjects.
740
741 As stated earlier, the visual evoked potentials, P1, N1, and P2, play a prominent role in the
742 brain's initial response to the object on the screen. Therefore, their spatial analysis is essential and
743 is given in Fig. 12. There are noticeable differences in the spatial profiles of EEG for NMC and

NVP subjects. The EEG potentials of P1 for NMC subjects show strong activity in a large area in the lower half of the plot, primarily in the visual, parietal, central, and left temporal regions. In comparison, for NVP subjects, it is mostly concentrated in visual, parietal, and central areas with a slight tilt toward the right side. The N1 positive potential activity for NMC subjects is distributed mainly in the left front and central areas, while for the NVP subjects, it is the left and right top portions of the plots. The negative components for both groups of subjects are distributed in the lower central and right areas. For NMC subjects, it is more focused, while for NVP subjects, it is distributed in larger areas in the lower right area of the plots. For the P2 potentials, both groups show some activity near the nose in the plots, which refers to the brain activity measured at electrodes on the forehead related to cortical activity in the frontal and orbital brain areas. The stark differences are evident in the lower posterior areas, where the NMC subjects exhibit less activity, while the NVP subjects show strong and distributed activity. There is a bright spot in the left frontal area for both groups of subjects.

Fig. 12. Spatial profiles of EEG, PSR1, and PSR2 for visual evoked response potentials, P1, N1, and P2 for NMC and NVP subjects. (Top row) EEG potentials in the broad (3-49 Hz), (middle row) PSR1, and (bottom row) PSR2. The PSR1 and PSR2 are in the alpha (7-12 Hz) band.

The spatial patterns for PSR1 (Fig. 12, middle row) are remarkably different from those of EEG potentials for all three peaks. For the P1 peak of NMC subjects, there is a bright spot near the right ear related to right temporal and auditory cortical brain activity. In contrast, for NVP subjects, there is a bright spot above the left ear, referring to the electrical activity of the left temporal and auditory cortices. Another noticeable difference in PSR1 plots is that NMC subjects have bright spots in the right frontal and central areas, which are missing for NVP subjects. This would suggest that there are some differences in the cortical activity of P1 peaks between NMC and NVP subjects. The PSR1 activity of the N1 peak is also different between NMC and NVP subjects. For the NMC subjects, it has bright spots near the right ear, right frontal, and left posterior central areas. In contrast, for the NVP subjects, PSR1 activity is distributed in the posterior region, near the right ear, and also exhibits some focused bright spots in the left central and parietal midline areas. There are also noticeable differences in the PSR1 plots of P2 peaks for NMC and NVP subjects. A noticeable difference is seen in the right front temporal and central posterior areas. The spatial plots of PSR2 have bright spots, which are well correlated with the bright spots in the PSR1 plots for all three peaks.

The *RDM** and *MAG* values were computed for a comparative analysis between NMC and NVP subjects for all three peaks. These are listed in Table 1. Here, the reference model is the NMC subjects, and the test model is the NVP subjects. As stated earlier, if the reference and test models are the same, then *RDM** will be zero and the *MAG* will be unity. From the values given in the table, it can be inferred that the EEG, PSR1, and PSR2 are significantly different for the NMC and NVP subjects across all three peaks.

Table 1. The *RDM** and *MAG* values for NMC and NVP subjects at the P1, N1, and P2 peaks.

	P1 Peak		N1 Peak		P2 Peak	
	*RDM**	*MAG*	*RDM**	*MAG*	*RDM**	*MAG*
EEG	0.486	1.585	0.976	0.866	0.673	2.290
PSR1	0.849	0.943	0.656	1.430	0.687	1.025
PSR2	0.768	0.880	0.705	0.985	0.635	0.869

D.5 Time Frames of Insight Moments for NMC and NVP Subjects

There are several stages involved in recognizing the name and form of an object from memory [1], and our results indicate that there are subtle timing differences in these stages for NMC and NVP subjects. This is what we are investigating in here. These different stages of insight moments have been described in the literature [1, 36, 49, 43]. Stage I is the first impression of the object in the visual cortex, and it is called the "Awe" moment in the knowledge cycle. It is generally identified with the P1 wave of the visual evoked potentials. Stage II is related to the rapid exploration of the nature of the object in language and memory areas of the brain. The Stage III is the "Eureka" moment, also called the "Illumination" moment, when one recognizes

809 and identifies the object. The Stage IV is called the "Verification" stage [1] and it is related to the
810 integration of the new knowledge in the memory for immediate future use, such as in visual
811 object naming tasks. Stage V is the start of the return to the background activity of the brain.
812 These different stages for a frontocentral electrode potentials are marked in Fig. 13A. The EEG
813 potentials are in the 3-49 Hz band. Some of the prominent peaks are also marked, which are also
814 shown in Fig. 3A and Fig. 11.
815
816 --------
817 Fig. 13. (A) EEG potentials in the 3-49 Hz band for one of the electrodes in the
818 frontocentral areas and the associated phase slip rates, PSR1. Different stages of
819 the insight moments are also marked for NMC and NVP subjects. (B) Spatial
820 plots of EEG and PSR1 of their prominent peaks for NMC and NVP subjects, and
821 note their differences.
822 ---------
823
824 The initial first three stages of insight moments are similar, with only minor differences of a few
825 milliseconds for NMC and NVP subjects. However, the duration of the fourth (IV) and fifth (V)
826 stages is different. Stage I is from 0.0 s to the location of the P1 visual evoked potential. This will
827 be the first impression of the object in the visual cortex. In the knowledge cycle, it is also called
828 the ‘Awe’ moment [1, 43, 49]. The endpoint of stage II is where the P2 peak ends, which can be
829 well recognized in the visual evoked potentials given in Figs. 2 and 10. During this stage, there is
830 rapid exploration of the nature of the object in language and memory areas of the brain [1]. Stage

III (305–561 ms) is the “Eureka” moment, also called the “Illumination” moment, when one recognizes and identifies the object [1, 36].

Stage IV in the knowledge cycle is called the "Verification" stage, and it is related to integrating the new knowledge into memory [1]. The Stage IV for the NVP subjects is from 561 to 702 ms, i.e., with a duration of 141 ms. In contrast, the Stage IV duration for NMC subjects is longer, ranging from 561 ms to 831 ms, with a total duration of 270 ms. Stages III and IV are critical stages in the process of identifying and assimilating new knowledge into memory. NVP subjects seem to be quicker at assimilating new knowledge into memory than NMC subjects. This is also reflected in the bimodal shape of the PSR1 activity for NVP subjects (lower plot in Fig. 13A). *So, for NVP subjects, it takes 702 ms from the start of the stimulus to identify and assimilate the new knowledge into memory. In comparison, for the same task, it took 831 ms for NMC subjects.*

Stage V marks the beginning of a return to background brain activity [1, 43].

The additional prominent peaks during the knowledge cycle, identified in Fig. 13A, are N707, P787, and N905. The spatial plots of EEG (3-49 Hz) potentials and their respective PSR1 are given in Fig. 13 B. The spatial plots of the EEG potentials for NMC and NVP subjects are significantly different ($p < 0.01$), which was confirmed by the paired Student’s t-test. Spatial differences are also noticeable for these three peaks between NMC and NVP subjects. For the N707 peak, the RDM* and MAG between NMC and NVP subjects were: 0.697 and 1.19. The same comparative values for the peak P787 were: 0.787 and 1.03. For the peak N905, these were:

853 0.85 and 1.29. These values suggest that the spatial plots of PSR1 for the NMC and NVP
854 subjects are significantly different from each other.
855
856 **E. Discussions**
857
858 Our primary objective was to quantify the differences in decision-making processes between
859 NMC and NVP subjects. Our results demonstrate quantifiable differences in four biomarkers that
860 we utilized in this study. The temporal and spatial patterns of EEG, EEG′, PSR1, and PSR2
861 indicate that different brain regions are activated in NMC and NVP subjects. Another remarkable
862 finding is that NVP subjects are quicker (702 ms) compared to NMC subjects (831 ms) in
863 completing the visual task of identifying and assimilating new knowledge into memory. This is a
864 remarkable finding that suggests people can be trained to perform tasks more efficiently for
865 visual object recognition. Similar results may also be observed in other tasks, such as motor
866 function-related tasks, which should be examined through carefully designed studies comparing
867 NMC subjects with those who have undergone meditative training.
868
869 Although many studies have been conducted to examine the efficacy of Vipassana in the context
870 of mindfulness-based interventions, relatively few studies have focused on traditional Vipassana
871 practitioners. Prior work from our group has examined EEG profiles of three proficiency-linked
872 groups of Vipassana meditation practitioners while they engaged in a structured sequence of
873 meditation practice (Anapana or focused attention, Vipassana or mindfulness, and Metta or
874 loving-kindness) and found that long-term meditators (seniors and teachers) showed widespread

875 trait and state differences as compared to novice meditators [28]. Examination of P300 dynamics
876 in the same three groups of meditators during the performance of the ANGEL task had revealed
877 significant state-trait influences of meditation practice [29]. Future work could therefore evaluate
878 the applicability of the four biomarkers employed in the current study across distinct meditation
879 states in NVPs and in long-term meditators.
880
881 Our work with novice Vipassana-trained subjects was facilitated by the availability of their data
882 sets and can be readily applied to other datasets from Vipassana meditators [50]. However, the
883 techniques and tools developed for this work are generic and versatile, and can be potentially
884 applied to any EEG data set to augment the existing set of measures. For instance, these tools can
885 be used to study the behavior of default mode networks in the spontaneous EEG or evoked
886 potential studies [51]. Similarly, our tools are applicable across diverse meditation practices,
887 including Zen, Mindfulness, Insight, other Buddhist and non-Buddhist traditions [52, 53, 54, 55].
888 Indeed, recent work examining EEG data from four different meditation traditions revealed both
889 a common core and tradition-specificity in the neurodynamic profiles [56]. When the mind is
890 trained to remain stable and focused, tools from our current work can augment traditional
891 measures in detecting subtle changes in brain activity from EEG data [57, 58]. Their sensitivity
892 extends to calm-abiding practices that cultivate stability and insight (Samatha & Vipassana) and
893 to practices that foster compassion, generosity, morality, joyous effort, and loving-kindness [59,
894 60, 61]. We hope that other investigators will adopt these tools in their research work.
895

We have used four biomarkers in this study. The spatial profiles of EEG and EEG′ are similar, with some minor differences which are not significant. Similarly, the spatial differences in the PSR1 and PSR2 plots are also minor. However, there are some significant differences between the spatial plots of EEG and its related PSR1, as well as between EEG′ and PSR2, that require explanation. Refer to Figs. 6 and 8. We first introduced these biomarkers in our recent work [4], where we mentioned that the first-order derivative of the EEG data removes linear trends and amplifies nonlinear trends and oscillatory activity in the data. The computation of the phase from EEG or EEG′ by use of the Hilbert transform does not depend upon the amplitude of the data but rather on large and small perturbations in the data. Even at the small perturbations in the data, a $\pm\pi$ phase shift is introduced, which could influence the computations of PSR1 and PSR2 at numerous spatial locations. Additionally, within a given time slice of the EEG (or EEG′) data, large amplitude values may occur on a few channels, while small perturbations in the data may occur on other channels. Thus, the spatial locations of PSR1 and PSR2 could be different from the spatial locations of EEG or EEG′, respectively. These could be the reasons why the EEG and PSR1, as well as EEG′ and PSR2, show some significant differences in the spatial plots. One could verify these by source location analysis from EEG and PSR1, or from EEG' and PSR2. This is a significantly big task, perhaps suitable for a separate study.

Our results, in line with earlier research [4], underscore the robustness of phase slip activity across broader brain areas, even when EEG potentials are low or near the zero-crossing lines. This robustness suggests that phase slip rates could be a more sensitive biomarker than EEG or EEG′ for detecting changes in brain activity. Importantly, this could significantly enhance our

918 understanding of brain functions, particularly in scenarios such as the study of the EEG of
919 anesthetized patients [62], the EEG data of subjects engaged in the Tukdum practice of Buddhist
920 meditation near the time of death [63], or the EEG of subjects going through near-death
921 experiences [64]. In these situations, the use of phase slip rate biomarkers derived from EEG, as
922 well as the first and second-order derivatives of EEG, could provide valuable insights into brain
923 activity, where EEG alone may not be sensitive enough to detect widespread changes in brain
924 activity [4]. Furthermore, phase slip rates could serve as a sensitive gauge to monitor the level of
925 anesthesia or the patient's level of consciousness during surgery or meditation.
926
927 Here, we have limited our work to the alpha (7-12 Hz) band only, which, in general, is the most
928 predominant band in the power spectrum and also plays a crucial role in visual object recognition
929 and insight moment analysis studies [1]. In future studies, this work could be extended to other
930 EEG bands, such as theta, alpha, beta, and gamma bands, which may provide additional insights
931 into the similarities and differences between NMC and NVP subjects in decision making
932 processes. Additionally, phase amplitude couplings between different bands, such as theta-alpha
933 or beta-gamma bands, may be another area to explore.
934
935 In summary, we demonstrated that cortical phase transitions alter during decision making and
936 that brain functions differ between non-meditators and novice Vipassana meditators. These
937 methods and results may aid future experimental designs in visual cognition and mindfulness
938 research, as well as contribute to educational neuroscience and the development of
939 neurofeedback technologies for clinical applications. This is our hope.

F. Data availability statement

Publicly available data sets were used in this study. This data can be found at: https://osf.io.

G. Author contributions

RJK: Conceptualization, Methodology, Writing – original draft, Writing – review & editing.

AKN: Data curation, Data analysis, Writing – original draft, Writing – review & editing.

AS: Data curation, Data analysis, Writing – review & editing.

RV: Data Curation.

PNR: Project administration, Supervision, Writing – review & editing.

BK: Project administration, Supervision, Writing – review & editing.

CR: Conceptualization, Methodology, Data curation, Data analysis, Software, Visualization, Writing – original draft, Writing – review & editing.

H. Funding

No funding for this project

I. Conflict of interest

961 The authors declare that the research was conducted in the absence of any commercial or

962 financial relationships that could be construed as a potential conflict of interest.

963

964 **Figure Captions**

965

966 Fig. 1. Schematic representation of the Vipassana practice in the tradition of Sayagyi U Ba Khin
967 as taught by S.N. Goenka.

968

969 Fig. 2. Protocol Diagram from earlier publication. Representative examples from two types of
970 task blocks. (From Nair et al., 2016).

971

972 Fig. 3. An example of an EEG trace after preprocessing for two electrodes in a 3-49 Hz
973 broadband. (A) EEG from one of the electrodes in the frontocentral area, (B) EEG from
974 one of the electrodes in the right visual area, and (C) spatial profile of EEG potentials at
975 the P1 peak of the NVP subject. Note that the time series profiles of PSRs at two
976 electrodes are significantly different during the 0.0-1.0 s period, when the subject is
977 visualizing and analyzing the image of the object during covert object naming tasks.

978

979 Fig. 4. A pictorial representation of phase slip extraction steps. Plots in the left column are
980 marked in (A) for the phase slips extraction from the EEG, and, similarly, the right
981 column (B) is for the phase slips extraction from EEG′, i.e., from the first order
982 derivative of EEG. The top row is the EEG and EEG′, the second row from the top is the
983 sawtooth pattern of the phase, the third row from the top is the unwrapped phase, and the
984 bottom row shows some of the phase slips.

985

986 Fig. 5. Temporal plots of quantities of one of the electrodes in the front central area for non-
987 meditator control (NMC) subjects. (Top left) EEG in 3-49 Hz band, (top right) EEG′ in
988 3-49 Hz band, (middle left) EEG filtered in the alpha band of 7-12 Hz, (middle right)
989 EEG′ filtered in the alpha band of 7-12 Hz, (bottom left) phase slip rate PSR1 extracted
990 from EEG in the alpha band, and (bottom right) phase slip rate PSR2 extracted from
991 EEG′ in the alpha band. Notice the prominent peaks in PSR1 and PSR2 related to brain
992 activity during the visual object recognition tasks. The prestimulus period is from -1.0 to
993 0.0 s. The combined stimulus and poststimulus period, referred to as the poststimulus+
994 period, spans from 0.0 to 2.0 seconds.
995
996 Fig. 6. Spatiotemporal plots of the root mean square (RMS) values of EEG and its first order
997 derivative (EEG′) and their associated mean values of phase slip rates for non-meditator
998 control (NMC) subjects. The RMS and mean values were computed within a 0.5 s
999 stepping window. The temporal duration for each frame is given at the top. (A) The top
1000 two rows are for the RMS EEG and the mean PSR1, respectively. (B) The bottom two
1001 rows are for the RMS EEG′ and the mean PSR2. Notice the shifting spatial patterns of all
1002 four quantities.
1003
1004 Fig. 7. Temporal plots of quantities of one of the electrodes in the front central area for novice
1005 Vipassana (NVP) subjects. (Top left) EEG in 3-49 Hz band, (top right) EEG′ in 3-49 Hz
1006 band, (middle left) EEG filtered in the alpha band of 7-12 Hz, (middle right) EEG′
1007 filtered in the alpha band of 7-12 Hz, (bottom left) phase slip rate PSR1 extracted from

1008 EEG in the alpha band, and (bottom right) phase slip rate PSR2 extracted from EEG′ in
1009 the alpha band. Notice the prominent peaks in PSR1 and PSR2 related to brain activity
1010 during the visual object recognition tasks.
1011
1012 Fig. 8. Spatiotemporal plots of the root mean square (RMS) values of EEG and EEG′ and their
1013 associated mean values of phase slip rates for novice Vipassana (NVP) subjects. The
1014 RMS and mean values were computed in the stepping window of 0.5 s duration. The
1015 temporal duration for each frame is given at the top. (A) The top two rows are for the
1016 RMS EEG and the mean PSR1, and (B) the bottom two rows are for the RMS EEG′ and
1017 the mean PSR2, respectively. Notice the shifting spatial patterns of all four quantities
1018 from Frame 1 to Frame 6.
1019
1020 Fig. 9. (A) Spatial plots of RMS EEG above the baseline of NMC and NVP subjects, (B)
1021 corresponding spatial plots of mean PSR1 above the baseline, (C) histogram distribution
1022 of RMS EEG values shown in spatial plots of A, and (D) histogram distribution of
1023 PSR1values shown in spatial plots of B.
1024
1025 Fig. 10. (A) Spatial plots of RMS EEG′ above the baseline of NMC and NVP subjects,
1026 (B) corresponding spatial plots of mean PSR2 above the baseline, (C) histogram
1027 distribution of the RMS EEG′ values shown in spatial plots of A, and (D)
1028 histogram distribution of PSR2 values shown in spatial plots of B.
1029

Fig. 11. EEG potentials in the broad (3-49 Hz) band and corresponding phase slip rates in the alpha (7-12 Hz) at one of the electrodes in the right visual cortex. (Top) EEG potentials with prominent P1, N1, and P2 peaks marked, (middle) corresponding PSR1, and (bottom) corresponding PSR2. Notice the subtle differences in EEG peaks and remarkable differences in PSR1 and PSR2 between NMC and NVP subjects.

Fig. 12. Spatial profiles of EEG, PSR1, and PSR2 for visual evoked response potentials, P1, N1, and P2 for NMC and NVP subjects. (Top row) EEG potentials in the broad (3-49 Hz) band, (middle row) PSR1, and (bottom row) PSR2. The PSR1 and PSR2 are in the alpha (7-12 Hz) band.

Fig. 13. (A) EEG potentials in the 3-49 Hz band for one of the electrodes in the frontocentral areas and the associated phase slip rates, PSR1. Different stages of the insight moments are also marked for NMC and NVP subjects. (B) Spatial plots of EEG and PSR1 of their prominent peaks for NMC and NVP subjects, and note their differences.

1048 **References**

1049

1050 1. Ramon C, Graichen U, Gargiulo P, Zanow F, Knösche TR, Haueisen J. Spatiotemporal
1051 phase slip patterns for visual evoked potentials, covert object naming tasks, and insight
1052 moments extracted from 256 channel EEG recordings. Front Integr Neurosci. 2023 Jun
1053 13;17: 1087976. doi: 10.3389/fnint.2023.1087976.

1054 2. Ramon C, Doud A, Holmes MD. Decrease in phase slip rates and phase cone structures
1055 during seizure evolution and epileptogenic activities derived from microgrid ECoG data.
1056 Curr Res Neurobiol. 2024 Feb 19;6: 100126. doi: 10.1016/j.crneur.2024.100126.

1057 3. Freeman WJ, Holmes MD, West GA, Vanhatalo S. Fine spatiotemporal structure of
1058 phase in human intracranial EEG. Clin Neurophysiol. 2006 Jun;117(6): 1228-43. doi:
1059 10.1016/j.clinph.2006.03.012.

1060 4. Ramon C, Gargiulo P. Phase slips extracted from derivatives of EEG data provide a
1061 deeper insight into the formation of cortical phase transitions. Front Integr Neurosci. 2025
1062 Feb 25;19: 1471120. doi: 10.3389/fnint.2025.1471120.

1063 5. Woodman GF. A brief introduction to the use of event-related potentials in studies of
1064 perception and attention. Atten Percept Psychophys. 2010 Nov;72(8): 2031-46. doi:
1065 10.3758/APP.72.8.2031.

1066 6. Kounios J, Fleck JI, Green DL, Payne L, Stevenson JL, Bowden EM, Jung-Beeman M.
1067 The origins of insight in resting-state brain activity. Neuropsychologia. 2008 Jan
1068 15;46(1): 281-91. doi: 10.1016/j.neuropsychologia.2007.07.013. Epub 2007 Jul 27.

1069 7. Cocchi L, Gollo LL, Zalesky A, Breakspear M. Criticality in the brain: A synthesis of
1070 neurobiology, models and cognition. Prog Neurobiol. 2017 Nov;158: 132-152. doi:
1071 10.1016/j.pneurobio.2017.07.002. Epub 2017 Jul 19.
1072 8. Heffern EFW, Huelskamp H, Bahar S, Inglis RF. Phase transitions in biology: from bird
1073 flocks to population dynamics. Proc Biol Sci. 2021 Oct 27;288(1961): 20211111. doi:
1074 10.1098/rspb.2021.1111. Epub 2021 Oct 20
1075 9. Wang SH, Siebenhühner F, Arnulfo G, Myrov V, Nobili L, Breakspear M, Palva S, Palva
1076 JM. Critical-like Brain Dynamics in a Continuum from Second- to First-Order Phase
1077 Transition. J Neurosci. 2023 Nov 8;43(45): 7642-7656. doi:
1078 10.1523/JNEUROSCI.1889-22.2023. Epub 2023 Oct 10.
1079 10. Bak P, Tang C, Wiesenfeld K. Self-organized criticality: An explanation of the 1/f noise.
1080 Phys Rev Lett. 1987 Jul 27;59(4): 381-384. doi: 10.1103/PhysRevLett.59.381.
1081 11. Dhar D. Self-organized critical state of sandpile automaton models. Phys Rev Lett. 1990
1082 Apr 2;64(14): 1613-1616. doi: 10.1103/PhysRevLett.64.1613.
1083 12. Holt AB, Kormann E, Gulberti A, Pötter-Nerger M, McNamara CG, Cagnan H, Baaske
1084 MK, Little S, Köppen JA, Buhmann C, Westphal M, Gerloff C, Engel AK, Brown P,
1085 Hamel W, Moll CKE, Sharott A. Phase-Dependent Suppression of Beta Oscillations in
1086 Parkinson's Disease Patients. J Neurosci. 2019 Feb 6;39(6): 1119-1134. doi:
1087 10.1523/JNEUROSCI.1913-18.2018. Epub 2018 Dec 14.
1088 13. di Santo S, Villegas P, Burioni R, Muñoz MA. Landau-Ginzburg theory of cortex
1089 dynamics: Scale-free avalanches emerge at the edge of synchronization. Proc Natl Acad

1090 Sci U S A. 2018 Feb 13;115(7): E1356-E1365. doi: 10.1073/pnas.1712989115. Epub
1091 2018 Jan 29.
1092 14. Tognoli E, Kelso JA. The metastable brain. Neuron. 2014 Jan 8;81(1): 35-48. doi:
1093 10.1016/j.neuron.2013.12.022.
1094 15. Kozma R, Freeman WJ. Cinematic Operation of the Cerebral Cortex Interpreted via
1095 Critical Transitions in Self-Organized Dynamic Systems. Front Syst Neurosci. 2017 Mar
1096 14;11: 10. doi: 10.3389/fnsys.2017.00010.
1097 16. Beggs JM, Timme N. Being critical of criticality in the brain. Front Physiol. 2012 Jun
1098 7;3: 163. doi: 10.3389/fphys.2012.00163.
1099 17. Freeman WJ, Vitiello G. Nonlinear brain dynamics as macroscopic manifestation of
1100 underlying many-body field dynamics. Phys. Life Rev. 2006; 3(2): 93–118. doi:
1101 10.1016/j.plrev.2006.02.001.
1102 18. Freeman WJ, Vitiello G. Vortices in brain waves. International Journal of Modern
1103 Physics B. 2010 Jul 10;24(17): 3269-95. doi: 10.1142/S0217979210056025.
1104 19. Ramon C, Holmes MD, Wise MV, Tucker D, Jenson K, Kinn SR. Oscillatory Patterns of
1105 Phase Cone Formations near to Epileptic Spikes Derived from 256-Channel Scalp EEG
1106 Data. Comput Math Methods Med. 2018 Nov 21;2018: 9034543. doi:
1107 10.1155/2018/9034543.
1108 20. Grossman, P. Mindfulness for Psychologists: Paying Kind Attention to the Perceptible.
1109 Mindfulness. 2010; 1: 87–97. doi: 10.1007/s12671-010-0012-7.

1110 21. Bishop SR, Lau M, Shapiro S, Carlson L, Anderson ND, Carmody J, Segal ZV, Abbey S,
1111 Speca M, Velting D, Devins G. Mindfulness: A Proposed Operational Definition. Clinical
1112 Psychology: Science and Practice. 2004; 11: 230-241. doi: 10.1093/clipsy.bph077.
1113 22. Walsh R. Meditation. In: Corsini RJ, editor. Handbook of innovative psychotherapy. New
1114 York: John Wiley & Sons Inc.; 2001. pp. 368-380.
1115 23. Attrey S, Joshi S, Bhatt V. Mindful path to psychological wellbeing: a comprehensive
1116 review. Journal of Behavioral and Cognitive Therapy. 2025; 35(4), 100537. doi:
1117 10.1016/j.jbct.2025.100537.
1118 24. Siegel DJ. Mindfulness training and neural integration: differentiation of distinct streams
1119 of awareness and the cultivation of well-being. Soc Cogn Affect Neurosci. 2007
1120 Dec;2(4): 259–63. doi: 10.1093/scan/nsm034.://doi.org/10.1093/scan/nsm034.
1121 25. Tang YY, Hölzel BK, Posner MI. The neuroscience of mindfulness meditation. Nat Rev
1122 Neurosci. 2015 Apr;16(4): 213-25. doi: 10.1038/nrn3916. Epub 2015 Mar 18.
1123 26. Awasthi B. Issues and perspectives in meditation research: in search for a definition.
1124 Front Psychol. 2013 Jan 10;3: 613. doi: 10.3389/fpsyg.2012.00613.
1125 27. Ivanovski B, Malhi GS. The psychological and neurophysiological concomitants of
1126 mindfulness forms of meditation. Acta Neuropsychiatr. 2007 Apr;19(2): 76-91. doi:
1127 10.1111/j.1601-5215.2007.00175.x.
1128 28. Kakumanu RJ, Nair AK, Venugopal R, Sasidharan A, Ghosh PK, John JP, Mehrotra S,
1129 Panth R, Kutty BM. Dissociating meditation proficiency and experience dependent EEG
1130 changes during traditional Vipassana meditation practice. Biol Psychol. 2018 May;135:
1131 65-75. doi: 10.1016/j.biopsycho.2018.03.004. Epub 2018

1132 29. Kakumanu RJ, Nair AK, Sasidharan A, John JP, Mehrotra S, Panth R, Kutty BM.
1133 State-trait influences of Vipassana meditation practice on P3 EEG dynamics. Prog Brain
1134 Res. 2019;244: 115-136. doi: 10.1016/bs.pbr.2018.10.027. Epub 2019 Jan 22.
1135 30. Goenka SN. The Discourse Summaries. Igatpuri, India: Vipassana Research Institute;
1136 1987.
1137 31. Goenka, S. N. (1991). Buddha's Path is to Experience Reality. Sayagyi U Ba Khin
1138 Journal. 1991; 109: 13.
1139 32. U Ba Khin S. The Essentials of Buddha-Dhamma in Meditative Practice. In: Sayagyi U
1140 Ba Khin. Onalaska, WA, USA: Vipassana Research Publications, Pariyatti Publishing;
1141 1991. pp. 12-22.
1142 33. Ñanamoli T. The Practice of Loving-Kindness (Metta): As Taught by the Buddha in the
1143 Pali Canon. In The Four Sublime States Contemplations on Love, Compassion,
1144 Sympathetic Joy, and Equanimity (BPS online). Kandy, Sri Lanka: Buddhist Publication
1145 Society. 1994; Retrieved on 25 August 2025,
1146 http://www.accesstoinsight.org/lib/authors/nanamoli/wheel007.html
1147 34. Wallas G. The Art of Thought. New York: Harcourt, Brace and Company; 1926. pp. 10.
1148 35. Gell-Mann M. The Quark and the Jaguar: Adventures in the Simple and the Complex.
1149 New York: W.H. Freeman; 1994. pp. 264–265.
1150 36. Sadler-Smith E. Wallas' Four-Stage model of the creative process: more than meets the
1151 eye?. Creativity Research Journal. 2015; 27(4): 342-352. doi:
1152 10.1080/10400419.2015.1087277.

1153 37. Kounios J, Beeman M. The cognitive neuroscience of insight. Annu Rev Psychol.
1154 2014;65: 71-93. doi: 10.1146/annurev-psych-010213-115154.
1155 38. Oh Y, Chesebrough C, Erickson B, Zhang F, Kounios J. An insight-related neural reward
1156 signal. Neuroimage. 2020 Jul 1;214: 116757. doi: 10.1016/j.neuroimage.2020.116757.
1157 Epub 2020 Mar 16.
1158 39. Salvi C, Bricolo E, Franconeri SL, Kounios J, Beeman M. Sudden insight is associated
1159 with shutting out visual inputs. Psychon Bull Rev. 2015 Dec;22(6): 1814-9. doi:
1160 10.3758/s13423-015-0845-0.
1161 40. Nair AK, Sasidharan A, John JP, Mehrotra S, Kutty BM. Assessing Neurocognition via
1162 Gamified Experimental Logic: A Novel Approach to Simultaneous Acquisition of
1163 Multiple ERPs. Front Neurosci. 2016 Jan 29;10: 1. doi: 10.3389/fnins.2016.00001.
1164 41. Delorme A, Makeig S. EEGLAB: an open source toolbox for analysis of single-trial EEG
1165 dynamics including independent component analysis. J Neurosci Methods. 2004 Mar
1166 15;134(1): 9-21. doi: 10.1016/j.jneumeth.2003.10.009.
1167 42. Davis JJ, Kozma R, Freeman WJ. Neurophysiological evidence of the cognitive cycle and
1168 the emergence of awareness. In: 2013 International Joint Conference on Awareness
1169 Science and Technology & Ubi-Media Computing (iCAST 2013 & UMEDIA 2013) 2013
1170 Nov 2 (pp. 149-157). IEEE. doi.: 10.1109/ICAwST.2013.6765425.
1171 43. Myers MH, Kozma R, Davis JJ, Ilin R. (2014). Phase cone detection optimization in EEG
1172 data. In: Proceedings of the 2014 international joint conference on neural networks
1173 (IJCNN). Piscataway, NJ: IEEE; 2014. pp. 2504–2511. doi:
1174 10.1109/IJCNN.2014.6889880

1175 44. Kobayashi K, Shibata T, Tsuchiya H, Akiyama T. Exclusion of the Possibility of "False
1176 Ripples" From Ripple Band High-Frequency Oscillations Recorded From Scalp
1177 Electroencephalogram in Children With Epilepsy. Front Hum Neurosci. 2021 Jun 15;15:
1178 696882. doi: 10.3389/fnhum.2021.696882.
1179 45. Ramon C, Holmes MD. Stochastic Behavior of Phase Synchronization Index and
1180 Cross-Frequency Couplings in Epileptogenic Zones during Interictal Periods Measured
1181 with Scalp dEEG. Front Neurol. 2013 May 16;4: 57. doi: 10.3389/fneur.2013.00057.
1182 46. Freeman WJ, Rogers LJ. Fine temporal resolution of analytic phase reveals episodic
1183 synchronization by state transitions in gamma EEGs. J Neurophysiol. 2002 Feb;87(2):
1184 937-45. doi: 10.1152/jn.00254.2001.
1185 47. Varela F, Lachaux JP, Rodriguez E, Martinerie J. The brainweb: phase synchronization
1186 and large-scale integration. Nat Rev Neurosci. 2001 Apr;2(4): 229-39. doi:
1187 10.1038/35067550.
1188 48. Lancaster G, Iatsenko D, Pidde A, Ticcinelli V, Stefanovska A. Surrogate data for
1189 hypothesis testing of physical systems. Physics Reports. 2018 Jul 18; 748: 1-60. doi:
1190 10.1016/j.physrep.2018.06.001.
1191 49. Lee JY, Lindquist KA, Nam CS. Emotional Granularity Effects on Event-Related Brain
1192 Potentials during Affective Picture Processing. Front Hum Neurosci. 2017 Mar 24;11:
1193 133. doi: 10.3389/fnhum.2017.00133.
1194 50. Cahn BR, Delorme A, Polich J. Occipital gamma activation during Vipassana meditation.
1195 Cogn Process. 2010 Feb;11(1): 39-56. doi: 10.1007/s10339-009-0352-1. Epub 2009 Dec
1196 16.

1197 51. Berkovich-Ohana A, Glicksohn J, Goldstein A. Studying the default mode and its
1198 mindfulness-induced changes using EEG functional connectivity. Soc Cogn Affect
1199 Neurosci. 2014 Oct;9(10): 1616-24. doi: 10.1093/scan/nst153. Epub 2013 Nov 4.
1200 52. Brefczynski-Lewis JA, Lutz A, Schaefer HS, Levinson DB, Davidson RJ. Neural
1201 correlates of attentional expertise in long-term meditation practitioners. Proc Natl Acad
1202 Sci U S A. 2007 Jul 3;104(27): 11483-8. doi: 10.1073/pnas.0606552104. Epub 2007 Jun
1203 27.
1204 53. Hinterberger T, Schmidt S, Kamei T, Walach H. Decreased electrophysiological activity
1205 represents the conscious state of emptiness in meditation. Front Psychol. 2014 Feb 17;5:
1206 99. doi: 10.3389/fpsyg.2014.00099.
1207 54. Lomas T, Ivtzan I, Fu CH. A systematic review of the neurophysiology of mindfulness on
1208 EEG oscillations. Neurosci Biobehav Rev. 2015 Oct;57: 401-10. doi:
1209 10.1016/j.neubiorev.2015.09.018. Epub 2015 Oct 9.
1210 55. Schoenberg PLA, Ruf A, Churchill J, Brown DP, Brewer JA. Mapping complex mind
1211 states: EEG neural substrates of meditative unified compassionate awareness. Conscious
1212 Cogn. 2018 Jan;57: 41-53. doi: 10.1016/j.concog.2017.11.003. Epub 2017 Nov 21.
1213 56. Shrimali P, Sasidharan A, Malipeddi S, Ventura B, Venugopal R, Nair A K, et al. Similar
1214 States, Different Paths: Neurodynamics of diverse meditation techniques. bioRxiv
1215 2025.06.20.660652 [Preprint] 2025 [cited 2025 August 28]. Available from:
1216 https://doi.org/10.1101/2025.06.20.660652
1217 57. Malipeddi S, Sasidharan A, Pinna Nagendra R, Mehrotra S, P John J, M Kutty B. Data
1218 from "Relaxed alertness in novice and advanced meditators – A neurophysiological and

1219 psychological study of Isha Yoga practices". Mindfullness. Zenodo; 2024 Oct;
1220 https://doi.org/10.5281/zenodo.13969788.
1221 58. Nair AK, Sasidharan A, John JP, Mehrotra S, Kutty BM. Just a minute meditation: Rapid
1222 voluntary conscious state shifts in long term meditators. Conscious Cogn. 2017 Aug;53:
1223 176-184. doi: 10.1016/j.concog.2017.06.002. Epub 2017 Jul 5.
1224 59. Huang C, Kaliman P, Epel ES, Saron CD. Insight meditation and telomere biology: The
1225 effects of intensive retreat and the moderating role of personality. Brain Behav Immun.
1226 2018 May;70: 233-245. doi: 10.1016/j.bbi.2018.03.003. Epub 2018 Mar 5. Erratum in:
1227 Brain Behav Immun. 2018 Oct;73: 736-737. doi: 10.1016/j.bbi.2018.07.015.
1228 60. Nair AK, John JP, Mehrotra S, Kutty BM. What contributes to wellbeing gains –
1229 proficiency or duration of meditation related practices?. International Journal of
1230 Wellbeing. 2018 Dec 8; 8(2). doi: 10.5502/ijw.v8i2.696.
1231 61. Sankar Sylapan B, Nair AK, Jayanna K, Mallipeddi S, Sathyanarayana S, Kutty BM.
1232 Meditation, well-being and cognition in heartfulness meditators - A pilot study.
1233 Conscious Cogn. 2020 Nov;86: 103032. doi: 10.1016/j.concog.2020.103032. Epub 2020
1234 Oct 20.
1235 62. Purdon PL, Sampson A, Pavone KJ, Brown EN. Clinical Electroencephalography for
1236 Anesthesiologists: Part I: Background and Basic Signatures. Anesthesiology. 2015
1237 Oct;123(4): 937-60. doi: 10.1097/ALN.0000000000000841.
1238 63. Lott DT, Yeshi T, Norchung N, Dolma S, Tsering N, Jinpa N, Woser T, Dorjee K, Desel
1239 T, Fitch D, Finley AJ, Goldman R, Bernal AMO, Ragazzi R, Aroor K, Koger J, Francis
1240 A, Perlman DM, Wielgosz J, Bachhuber DRW, Tamdin T, Sadutshang TD, Dunne JD,

1241 Lutz A, Davidson RJ. No Detectable Electroencephalographic Activity After Clinical
1242 Declaration of Death Among Tibetan Buddhist Meditators in Apparent Tukdam, a
1243 Putative Postmortem Meditation State. Front Psychol. 2021 Jan 28;11: 599190. doi:
1244 10.3389/fpsyg.2020.599190.
1245 64. Martial C, Fritz P, Gosseries O, Bonhomme V, Kondziella D, Nelson K, Lejeune N. A
1246 neuroscientific model of near-death experiences. Nat Rev Neurol. 2025 Jun;21(6):
1247 297-311. doi: 10.1038/s41582-025-01072-z. Epub 2025 Mar 31. Erratum in: Nat Rev
1248 Neurol. 2025 Aug;21(8):465. doi: 10.1038/s41582-025-01111-9.
1249
1250

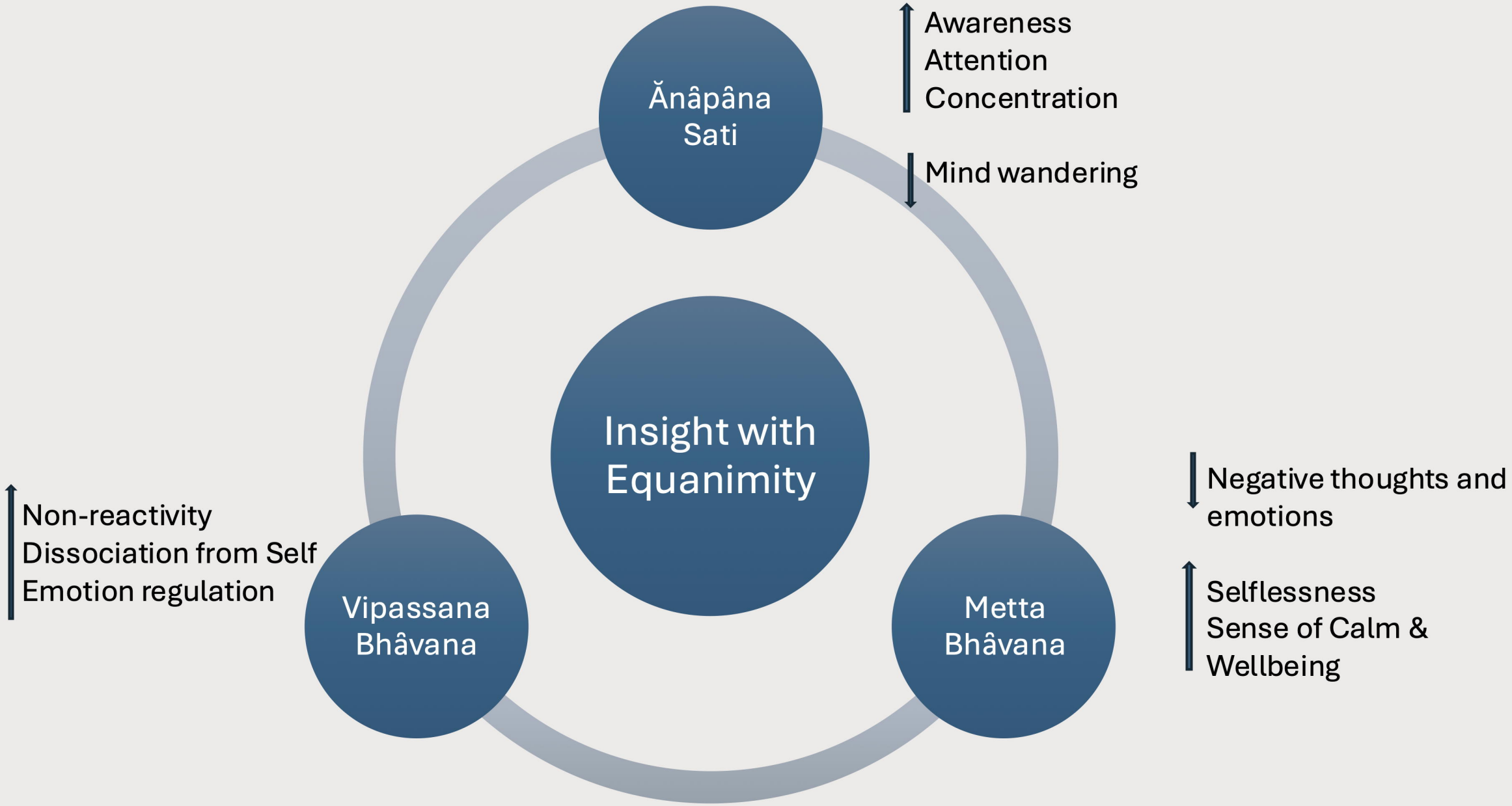
Ănâpâna Sati
Awareness
Attention
Concentration
Mind wandering
Insight with Equanimity
Negative thoughts and emotions
Selflessness
Sense of Calm & Wellbeing
Metta Bhâvana
Vipassana Bhâvana
Non-reactivity
Dissociation from Self
Emotion regulation

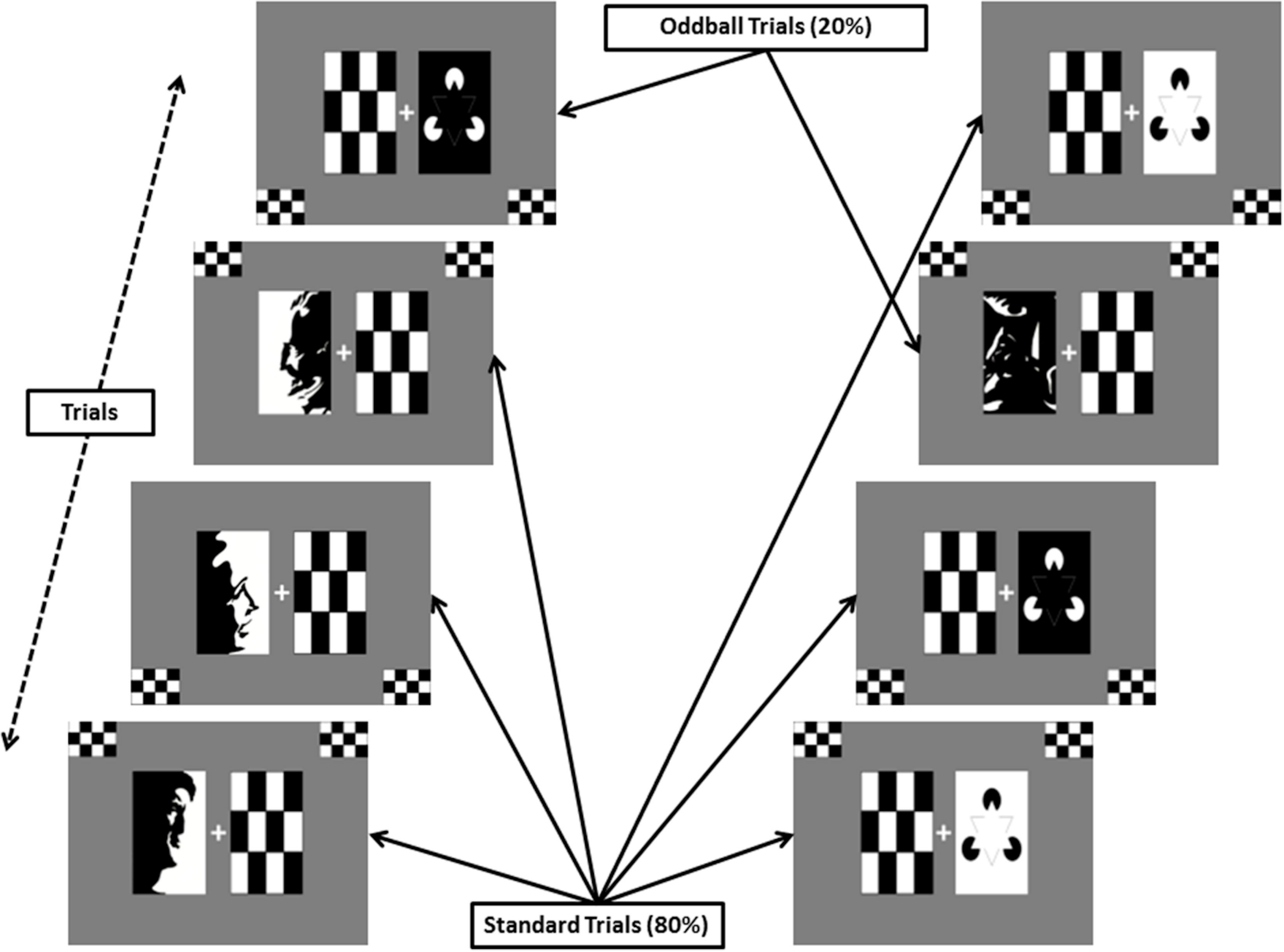
Oddball Trials (20%)
Trials
Standard Trials (80%)

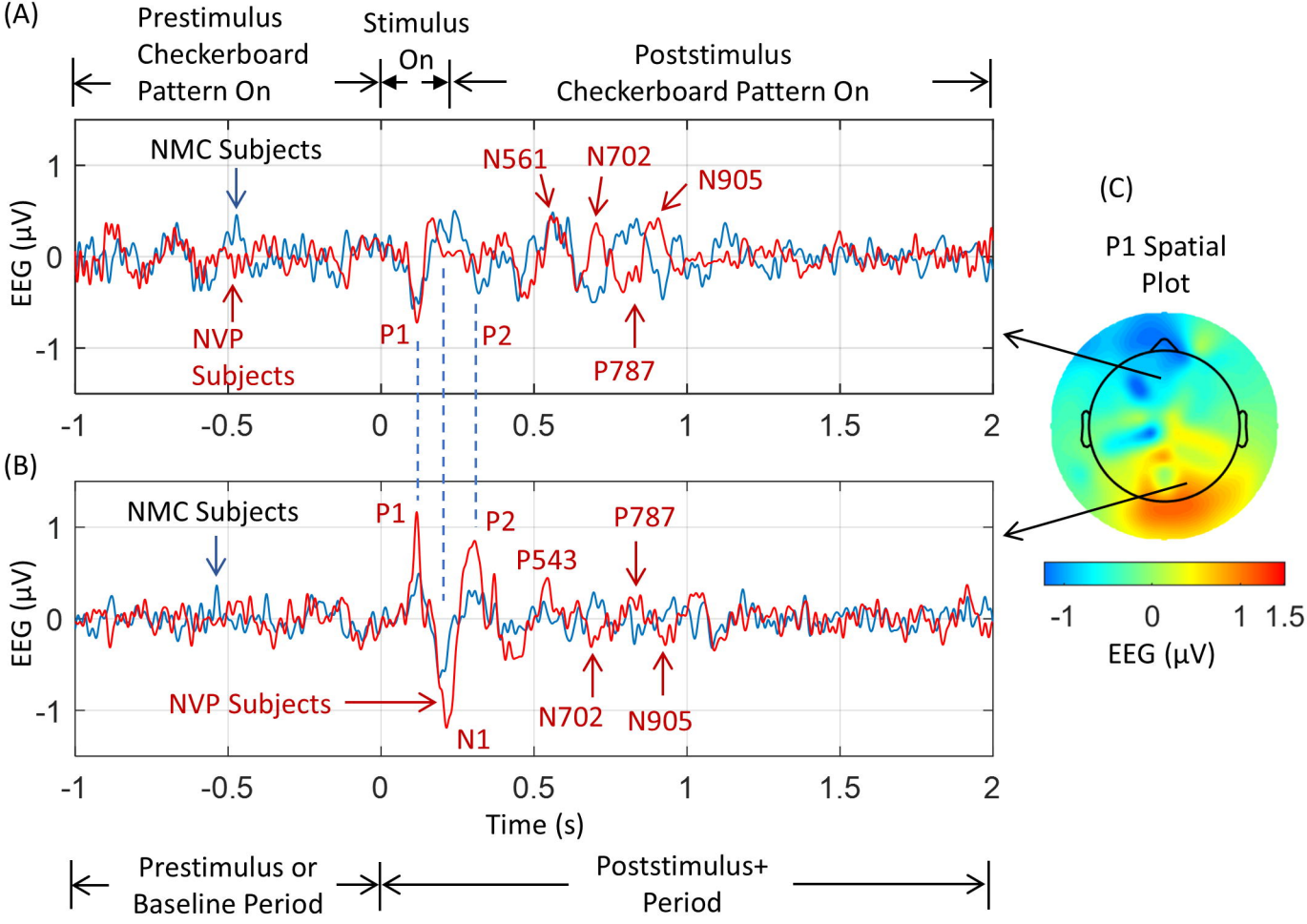
(A)
Prestimulus Checkerboard Pattern On
Stimulus On
Poststimulus Checkerboard Pattern On
NMC Subjects
N561
N702
N905
NVP Subjects
P1
P2
P787
EEG (μV)
(B)
NMC Subjects
P1
P2
P787
P543
NVP Subjects
N1
N702
N905
Time (s)
(C)
P1 Spatial Plot
EEG (μV)
Prestimulus or Baseline Period
Poststimulus+ Period

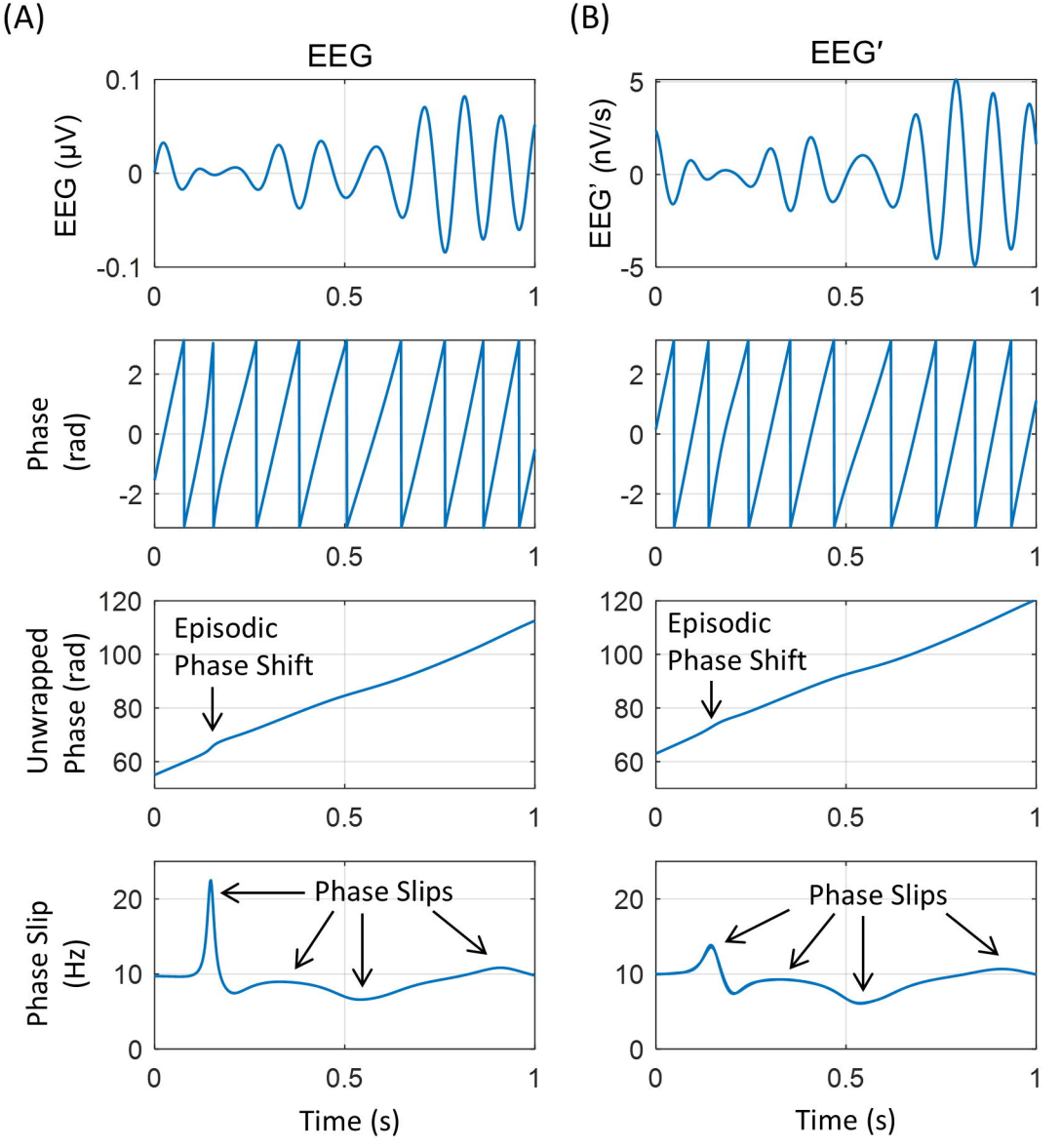
(A)
(B)
EEG
EEG′
EEG (μV)
EEG′ (nV/s)
Phase (rad)
Unwrapped Phase (rad)
Phase Slip (Hz)
Episodic Phase Shift
Phase Slips
Time (s)

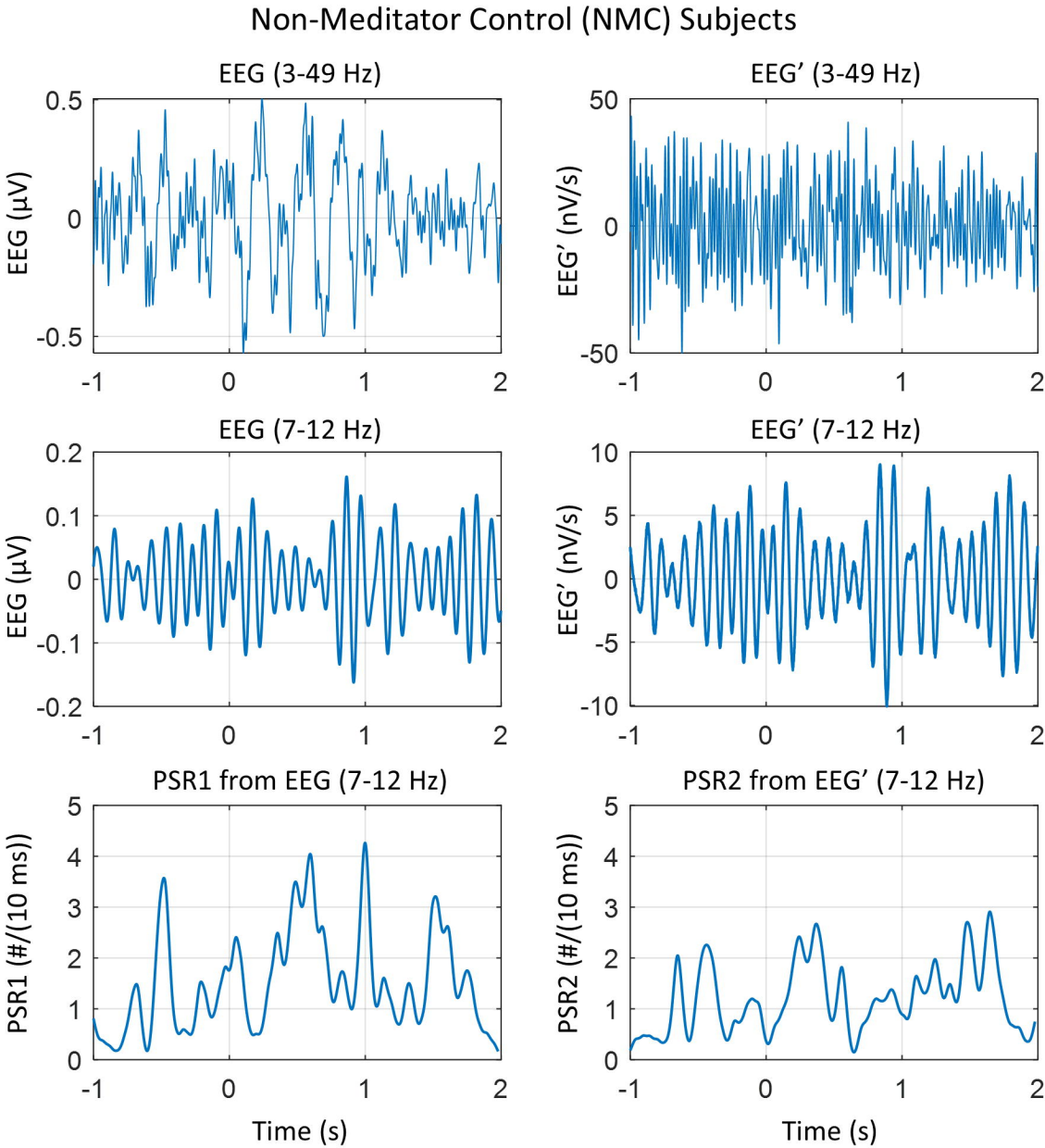
Non-Meditator Control (NMC) Subjects
EEG (3-49 Hz)
EEG (µV)
0.5
0
-0.5
-1
0
1
2
EEG' (3-49 Hz)
EEG' (nV/s)
50
0
-50
EEG (7-12 Hz)
0.2
0.1
-0.1
-0.2
EEG' (7-12 Hz)
10
5
-5
-10
PSR1 from EEG (7-12 Hz)
PSR1 (#/(10 ms))
PSR2 from EEG' (7-12 Hz)
PSR2 (#/(10 ms))
Time (s)

Non-Meditator Control (NMC) Subjects

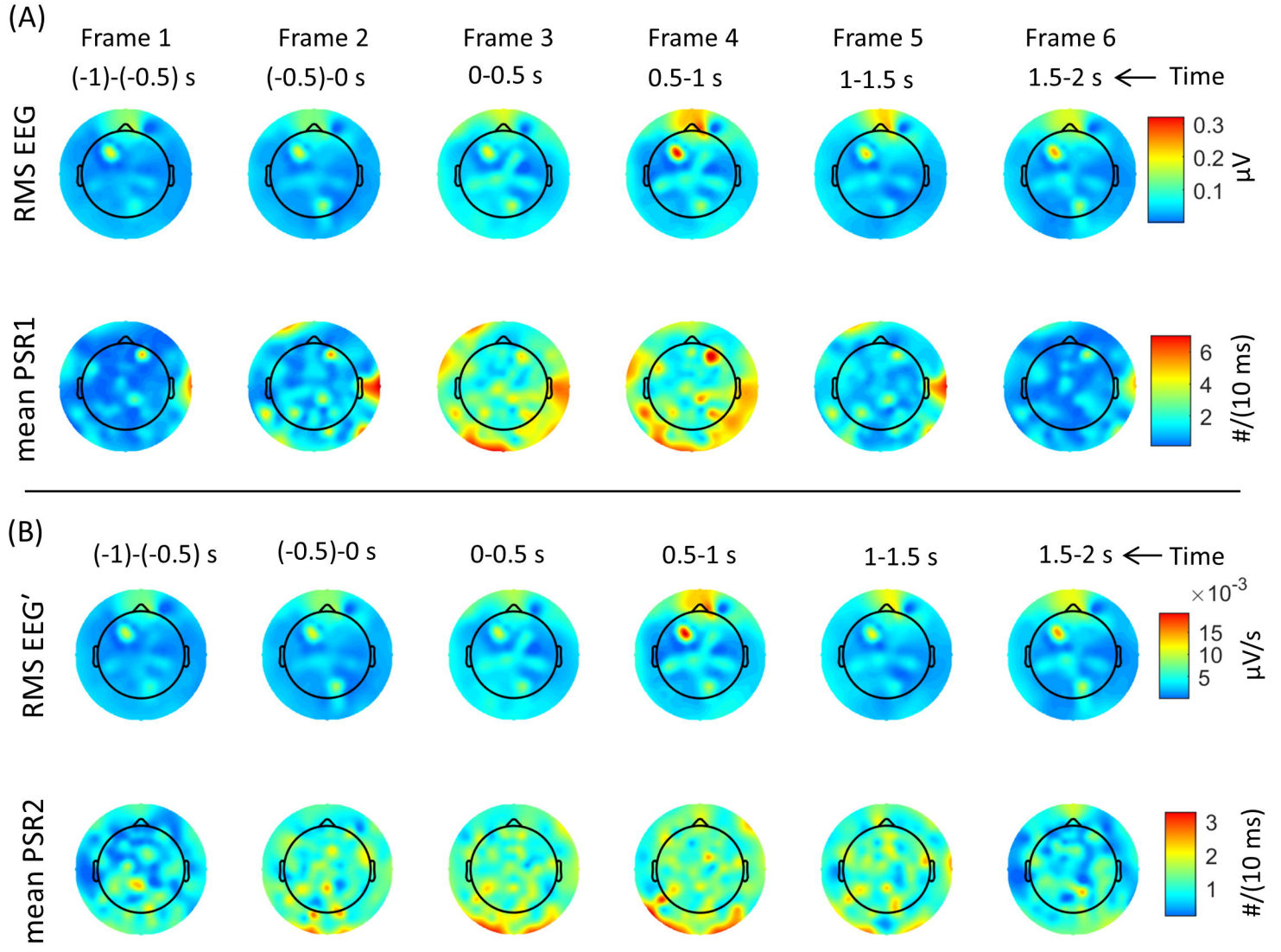

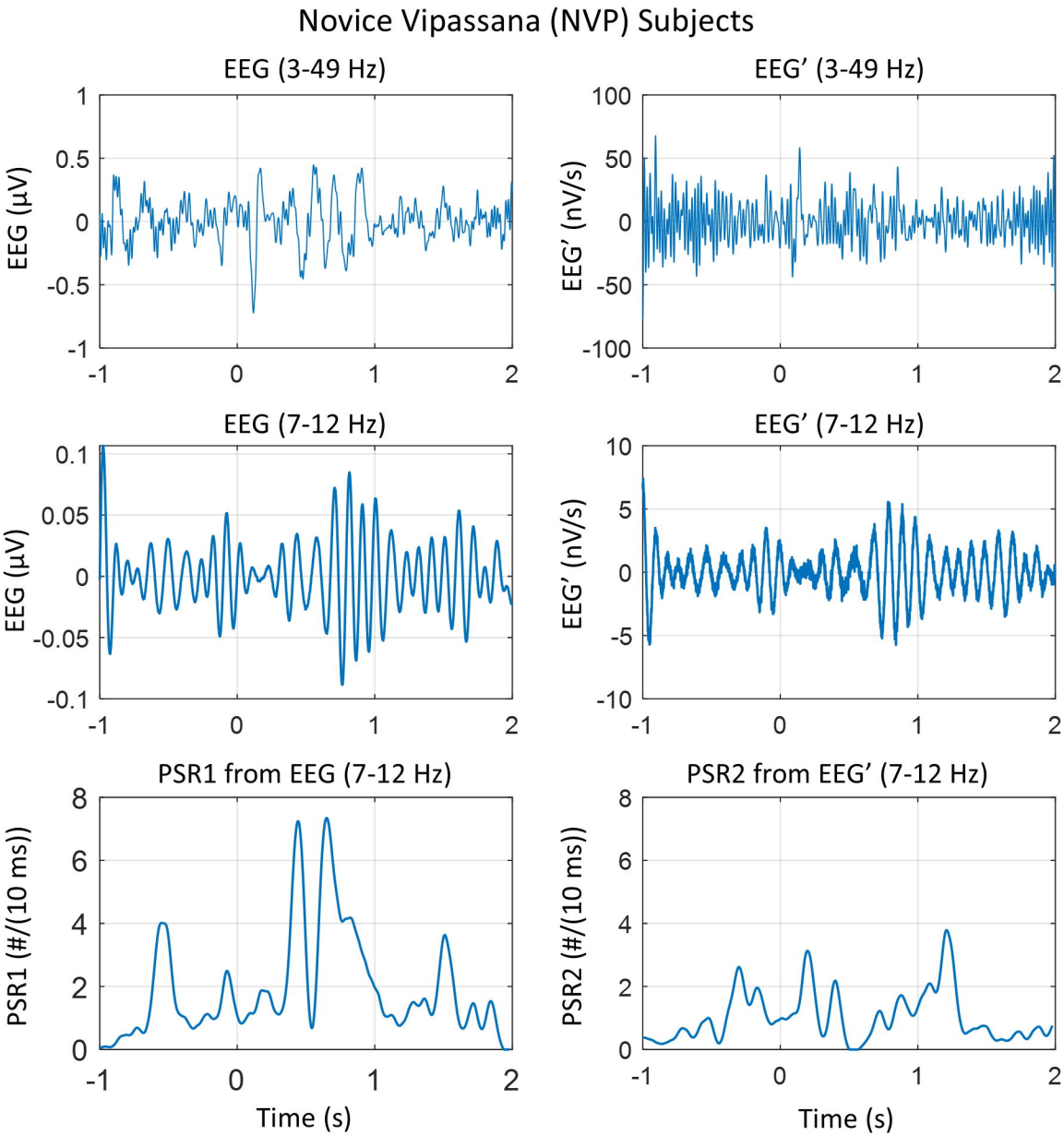
Novice Vipassana (NVP) Subjects
EEG (3-49 Hz)
EEG (μV)
EEG' (3-49 Hz)
EEG' (nV/s)
EEG (7-12 Hz)
EEG (μV)
EEG' (7-12 Hz)
EEG' (nV/s)
PSR1 from EEG (7-12 Hz)
PSR1 (#/(10 ms))
PSR2 from EEG' (7-12 Hz)
PSR2 (#/(10 ms))
Time (s)
Time (s)

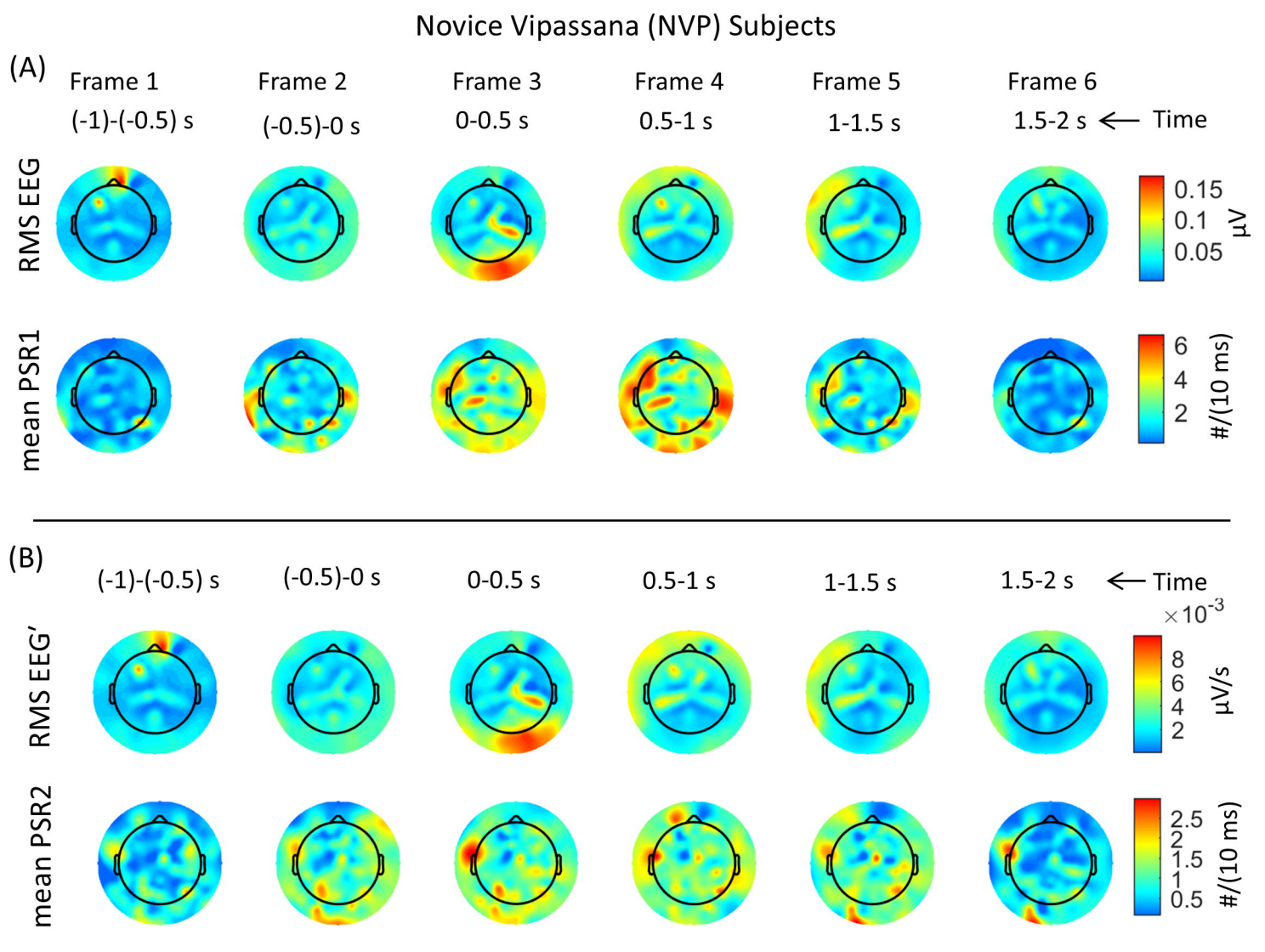
Novice Vipassana (NVP) Subjects
(A)
Frame 1
(-1)-(-0.5) s
Frame 2
(-0.5)-0 s
Frame 3
0-0.5 s
Frame 4
0.5-1 s
Frame 5
1-1.5 s
Frame 6
1.5-2 s
Time
RMS EEG
0.15
0.1
0.05
μV
mean PSR1
6
4
2
#/(10 ms)
(B)
(-1)-(-0.5) s
(-0.5)-0 s
0-0.5 s
0.5-1 s
1-1.5 s
1.5-2 s
Time
RMS EEG'
×10^-3
8
6
4
2
μV/s
mean PSR2
2.5
2
1.5
1
0.5
#/(10 ms)

RMS EEG and Mean PSR1 above Prestimulus Values

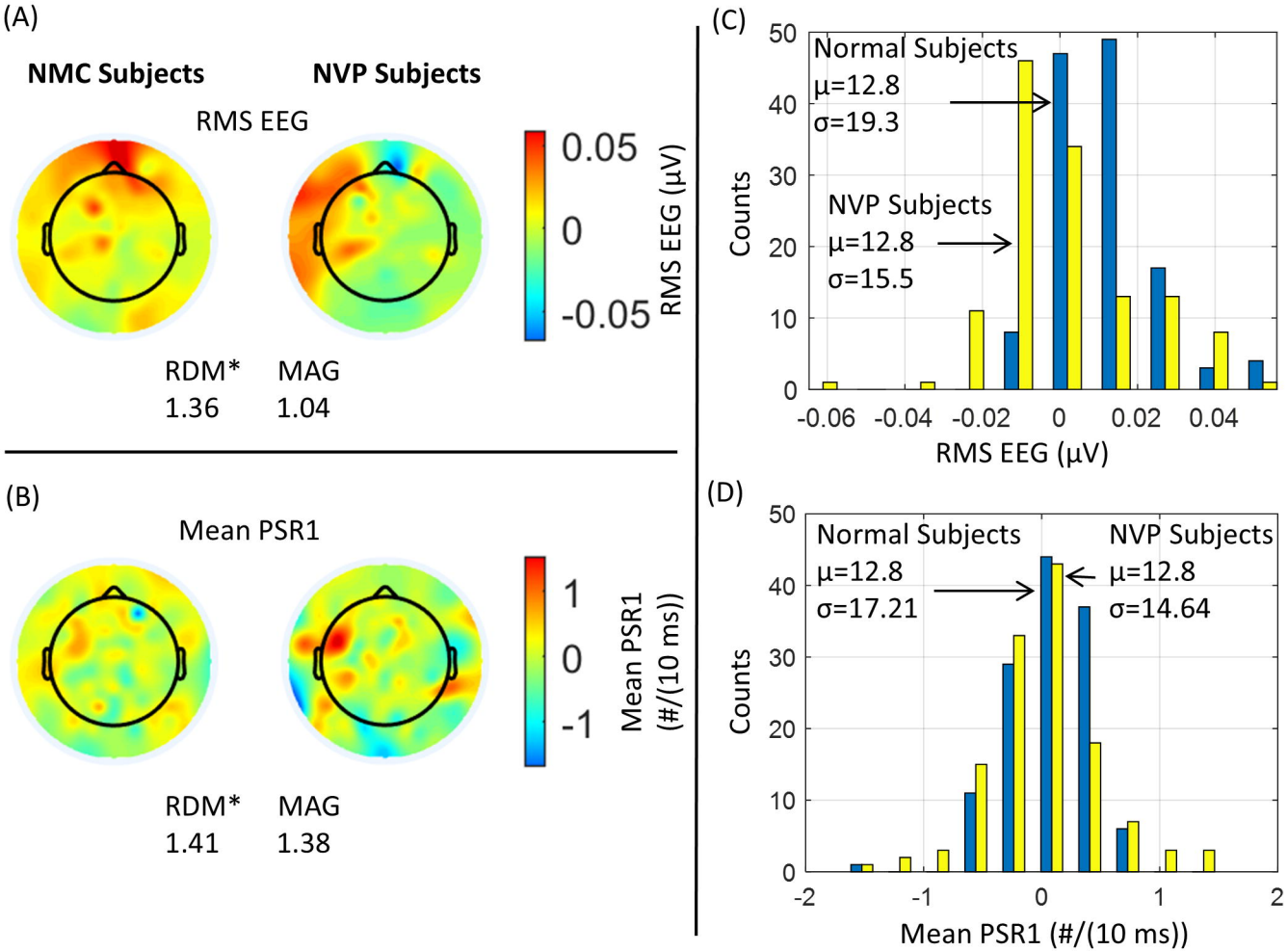

RMS EEG' and Mean PSR2 above Prestimulus Values

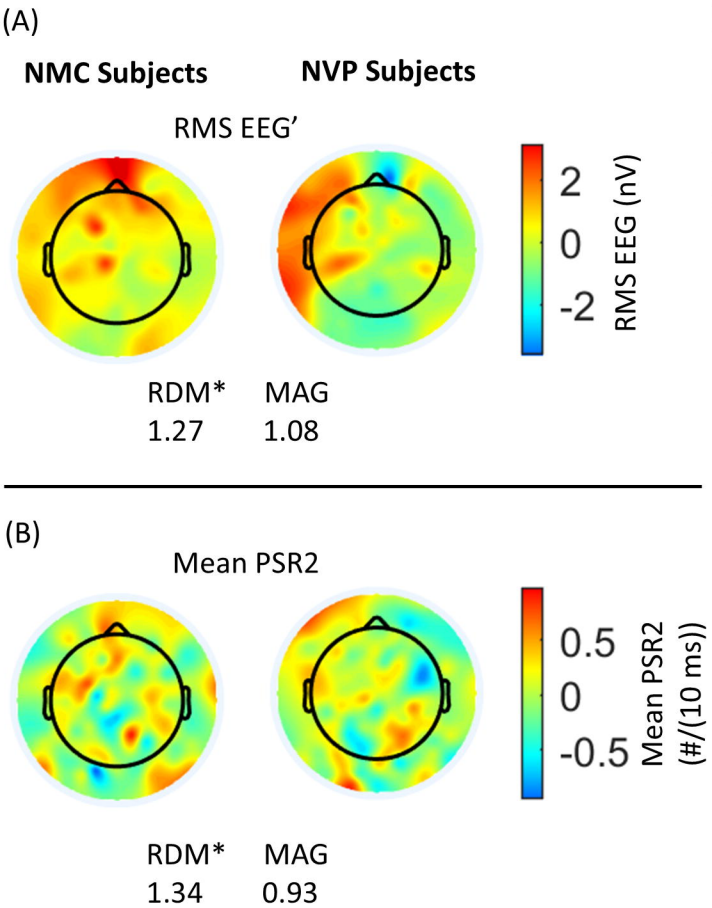

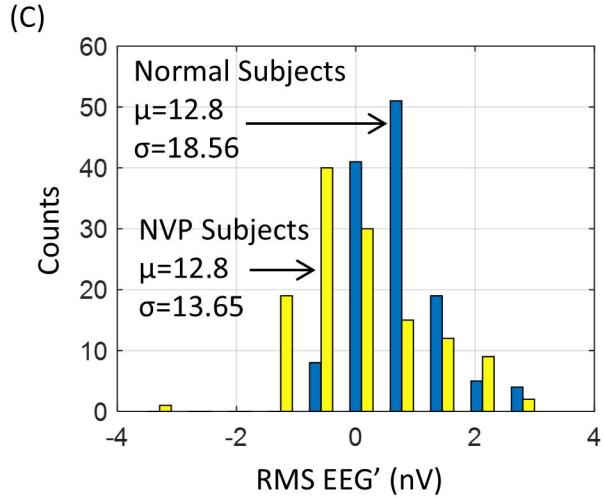

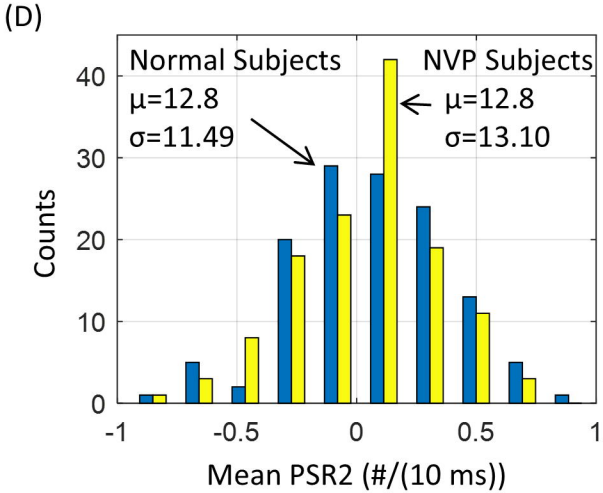

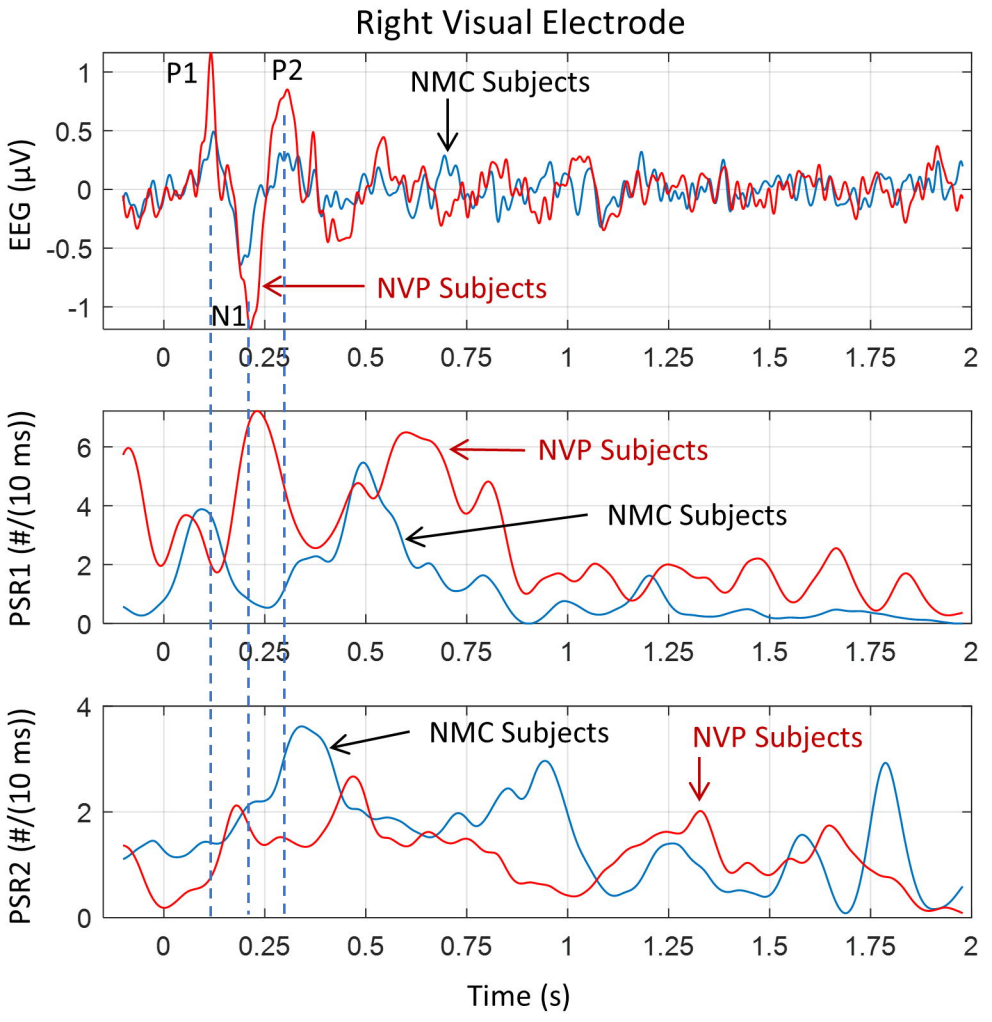
Right Visual Electrode
P1
P2
N1
NMC Subjects
NVP Subjects
EEG (μV)
1
0.5
0
-0.5
-1
0
0.25
0.5
0.75
1
1.25
1.5
1.75
2
PSR1 (#/(10 ms))
6
4
2
0
NVP Subjects
NMC Subjects
PSR2 (#/(10 ms))
4
2
0
NMC Subjects
NVP Subjects
Time (s)

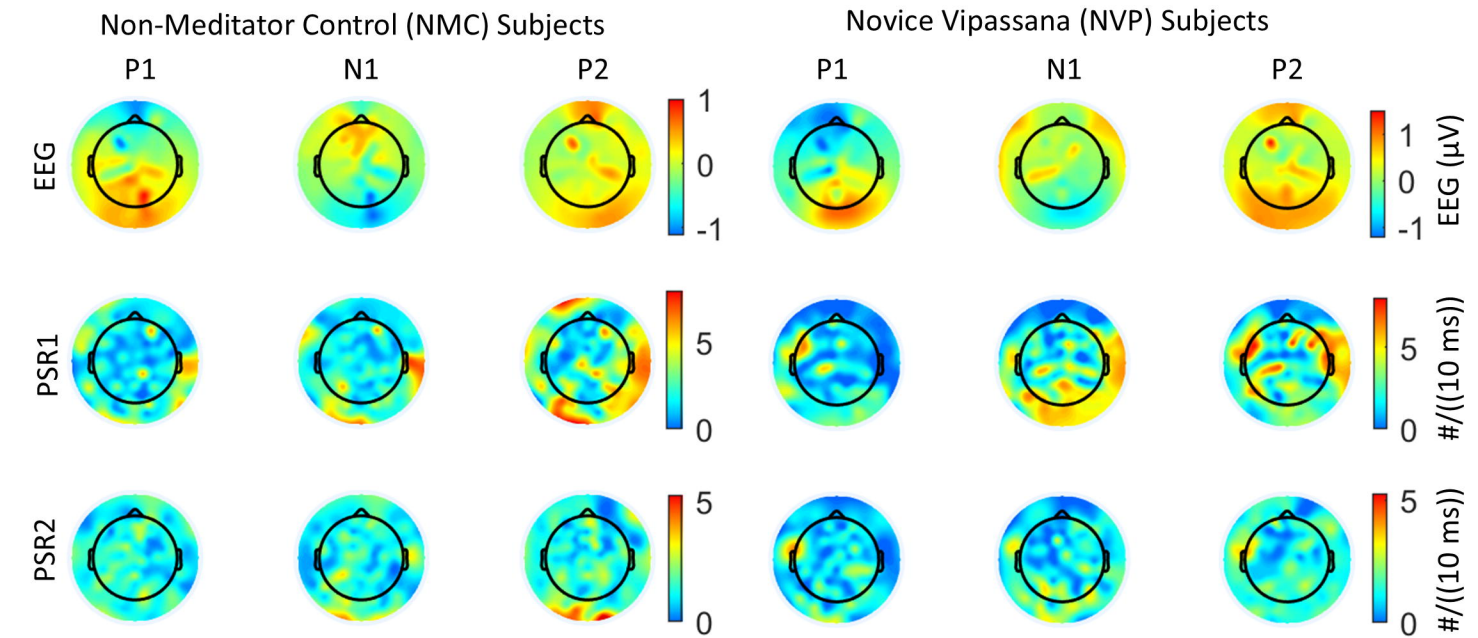
Non-Meditator Control (NMC) Subjects
Novice Vipassana (NVP) Subjects
P1
N1
P2
P1
N1
P2
EEG
PSR1
PSR2
1
0
-1
EEG (μV)
5
0
#/((10 ms))
5
0
#/((10 ms))

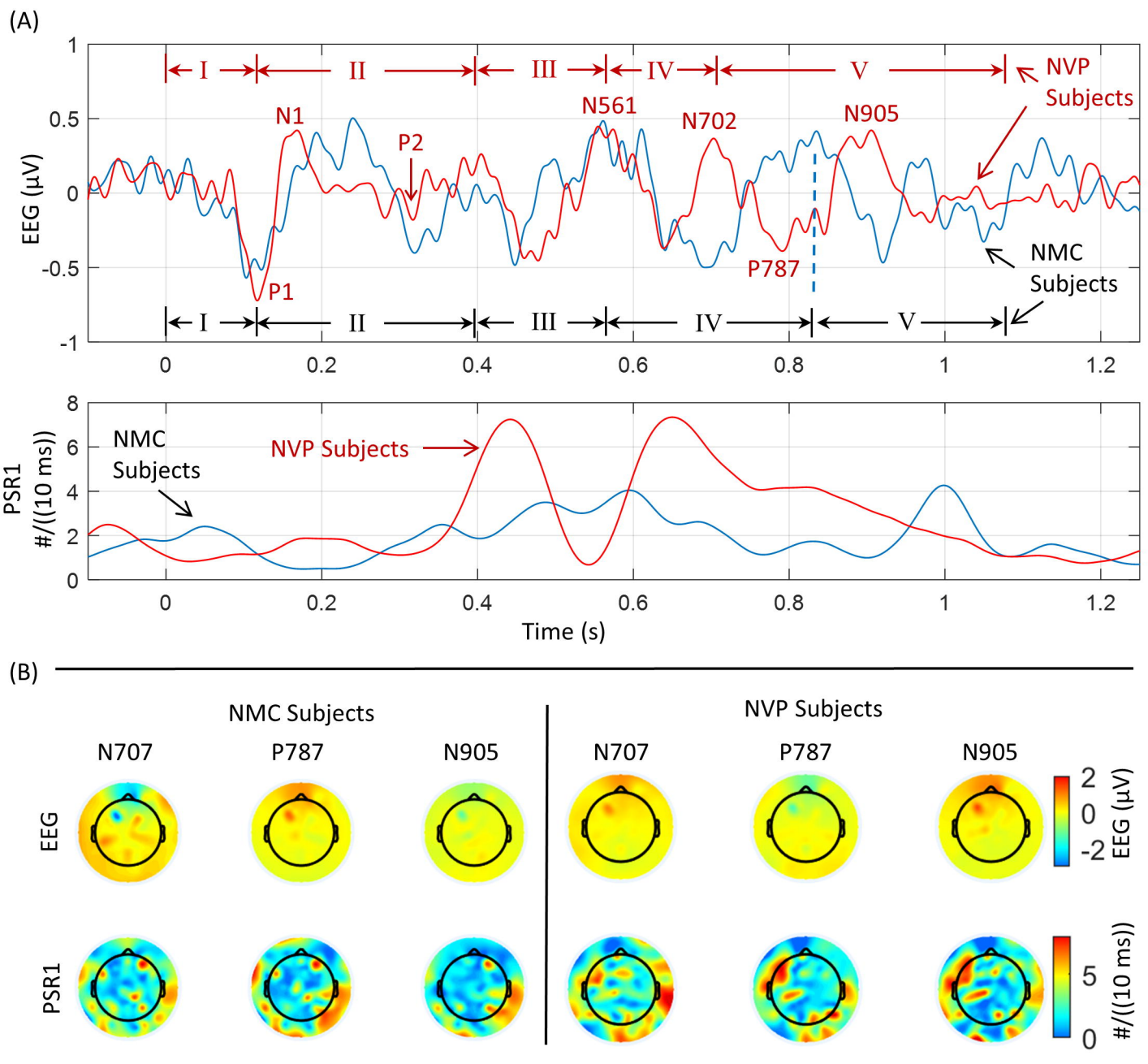
(A)
I
II
III
IV
V
NVP Subjects
N1
P2
N561
N702
N905
P1
P787
NMC Subjects
EEG (μV)
PSR1 #/((10 ms))
NMC Subjects
NVP Subjects
Time (s)
(B)
NMC Subjects
NVP Subjects
N707
P787
N905
EEG
PSR1
EEG (μV)
#/((10 ms))